



Article scientifique

Article

2023

Published version

Open Access

This is the published version of the publication, made available in accordance with the publisher's policy.

The ER stress sensor IRE1 interacts with STIM1 to promote store-operated calcium entry, T cell activation, and muscular differentiation

Carreras Sureda, Amado; Zhang, Xin; Laubry, Loann; Brunetti, Jessica; Konig, Stéphane; Wang, Xiaoxiao; Castelbou, Cyril; Hetz, Claudio; Liu, Yong; Frieden, Maud; Demaurex, Nicolas

How to cite

CARRERAS SUREDA, Amado et al. The ER stress sensor IRE1 interacts with STIM1 to promote store-operated calcium entry, T cell activation, and muscular differentiation. In: Cell reports, 2023, vol. 42, n° 12, p. 113540. doi: 10.1016/j.celrep.2023.113540

This publication URL: <https://archive-ouverte.unige.ch/unige:177196>

Publication DOI: [10.1016/j.celrep.2023.113540](https://doi.org/10.1016/j.celrep.2023.113540)

Article

The ER stress sensor IRE1 interacts with STIM1 to promote store-operated calcium entry, T cell activation, and muscular differentiation

Amado Carreras-Sureda,^{1,7,9,*} Xin Zhang,^{1,8} Loann Laubry,^{1,8} Jessica Brunetti,¹ Stéphane Koenig,¹ Xiaoxia Wang,² Cyril Castelbou,¹ Claudio Hetz,^{3,4,5} Yong Liu,⁶ Maud Frieden,¹ and Nicolas Demaurex^{1,7}

¹Department of Cell Physiology and Metabolism, University of Geneva, Geneva, Switzerland

²Shanghai Institute of Immunology, Department of Immunology and Microbiology, Shanghai Jiao Tong University School of Medicine, Shanghai Jiao Tong University, Shanghai, China

³Biomedical Neuroscience Institute (BNI), Faculty of Medicine, University of Chile, Santiago, Chile

⁴FONDAP Center for Geroscience (GERO), Brain Health and Metabolism, Santiago, Chile

⁵Program of Cellular and Molecular Biology, Institute of Biomedical Sciences, University of Chile, Santiago, Chile

⁶Hubei Key Laboratory of Cell Homeostasis, College of Life Sciences, the Institute for Advanced Studies, Wuhan University, Wuhan 430072, China

⁷These authors contributed equally

⁸These authors contributed equally

⁹Lead contact

*Correspondence: amado.carrerassureda@unige.ch

<https://doi.org/10.1016/j.celrep.2023.113540>

SUMMARY

Store-operated Ca^{2+} entry (SOCE) mediated by stromal interacting molecule (STIM)-gated ORAI channels at endoplasmic reticulum (ER) and plasma membrane (PM) contact sites maintains adequate levels of Ca^{2+} within the ER lumen during Ca^{2+} signaling. Disruption of ER Ca^{2+} homeostasis activates the unfolded protein response (UPR) to restore proteostasis. Here, we report that the UPR transducer inositol-requiring enzyme 1 (IRE1) interacts with STIM1, promotes ER-PM contact sites, and enhances SOCE. IRE1 deficiency reduces T cell activation and human myoblast differentiation. In turn, STIM1 deficiency reduces IRE1 signaling after store depletion. Using a CaMPARI2-based Ca^{2+} genome-wide screen, we identify CAMKG2 and *slc105a* as SOCE enhancers during ER stress. Our findings unveil a direct crosstalk between SOCE and UPR via IRE1, acting as key regulator of ER Ca^{2+} and proteostasis in T cells and muscles. Under ER stress, this IRE1-STIM1 axis boosts SOCE to preserve immune cell functions, a pathway that could be targeted for cancer immunotherapy.

INTRODUCTION

The endoplasmic reticulum (ER) is the major intracellular calcium (Ca^{2+}) store and site of synthesis of proteins with transmembrane domains or that are targeted to the secretory pathway.¹ Ca^{2+} in the lumen of the ER is maintained in the submillimolar range to facilitate protein folding in ionic conditions resembling the extracellular space, enabling the ER to act as a reservoir for Ca^{2+} signaling. When ER protein-folding capacities are overrun, cells undergo a state known as ER stress. Different conditions can induce ER stress including alterations in protein glycosylation, accumulation of misfolded proteins due the expression of aggregate-prone mutants, redox/oxidative imbalance, or disruption of ER Ca^{2+} homeostasis.² To overcome ER stress, cells engage the unfolded protein response (UPR), a cellular machinery composed of three major branches: the inositol-requiring enzyme 1 α (referred here as IRE1), the protein kinase R (PKR)-like ER kinase (PERK), and the activating transcription factor 6 α (ATF6 α), which act coordinately to determine cell fate under

ER stress. The UPR establishes adaptive and repair programs to improve folding and sustain cell function, but if the stress is not resolved, the UPR induces cell death.³ Importantly, chronic ER stress has been linked to the occurrence of several pathological processes including neurodegeneration, diabetes, and cancer.^{4,5}

The delicate equilibrium of ER Ca^{2+} luminal levels is maintained by the coordinated function of Ca^{2+} ion channels and pumps assembling at membrane contact sites (MCSs) between the ER and the plasma membrane (ER-PM) via a mechanism known as store-operated calcium entry (SOCE).⁶ When an agonist engages a PM receptor, it leads to secondary messenger signaling and the cleavage of phosphatidyl inositol (4,5) bisphosphate into inositol 1,4,5-trisphosphate (IP_3) and diacylglycerol. The burst in IP_3 in the cytosol opens inositol triphosphate receptors (ITPRs) in the ER membrane that release Ca^{2+} into the cytosol.⁷ This leads to a drop in luminal ER Ca^{2+} levels, which is sensed by stromal interacting molecule 1 (STIM1) via its EF-hand motif in the ER lumen.⁸ STIM1 then



unfolds into an extended conformation, oligomerizes, and migrates to cortical ER regions, forming MCSs with PM and appearing as puncta on the fluorescence microscope.^{9,10} Within MCSs, STIM1 gates the calcium release-activated calcium channel, encoded by *Orai1*, flooding the cytosol with this cation.^{11–13} This signaling is critical for T cell activation and proliferation¹⁴ and for muscle differentiation.^{15,16} Ca^{2+} is cleared from the cytosol via two main extrusion mechanisms, the PM Ca^{2+} -ATPase (PMCA) and the sarcoendoplasmic reticulum ATPase (SERCA) pump, which re-pumps Ca^{2+} into the ER, refolding the EF hand of STIM1 and ending SOCE.¹⁷

The ubiquitous SOCE pathway sustains ER luminal Ca^{2+} microenvironments and thus proteostasis in every cell. Indeed, for decades, researchers studying ER stress and SOCE have used the SERCA blocker thapsigargin (Tg) to activate ORAI1 currents or induce protein misfolding, suggesting that both events occur simultaneously following ER Ca^{2+} depletion. In yeast, alterations of ER-PM tethers induce ER stress and activate the UPR.¹⁸ The two pathways interact at the molecular level, as the ER stress transducer PERK was shown to coordinate ER-PM MCS formation via interactions with filamin A and actin polymerization.¹⁹ The UPR transducer IRE1 is a serine/threonine protein kinase and RNase that processes the mRNA encoding X-box binding protein-1 (XBP1), releasing a 26-nucleotide intron that acts as a transcription factor termed XBP1s, critical to engage adaptive programs.¹ IRE1 also degrades a subset of mRNAs through its RNase domain and activates alarm pathways by binding a series of adapter proteins.²⁰ In addition, IRE1 operates as a scaffold, interacting with several signaling proteins to regulate ER stress independent processes. IRE1 controls mitochondrial Ca^{2+} homeostasis and bioenergetics by regulating ITPR activity at ER-mitochondrial MCSs^{21,22} and drives cortical actin remodeling during cell migration by interacting with filamin A.²³ These observations indicate that IRE1 might also impact Ca^{2+} signaling at ER-PM contact sites, but surprisingly, the interactions between IRE1 and the STIM1/*Orai1* pathway have not been explored.

To unveil potential roles of IRE1 on calcium homeostasis, we performed a liquid chromatography and mass spectrometry (LC/MS) analysis in cells expressing or deficient for IRE1 that pointed us toward a dysregulation of STIM1 proteins. Since we previously showed that IRE1 promotes ITPR activity and this precludes STIM1 when SOCE is engaged, we studied the possible role of IRE1 on ER-PM contact formation and SOCE. We show that independently of the ITPR pathways, IRE1 directly interacts with STIM1 within the ER lumen to promote ER-PM contact assembly, STIM1-*Orai1* interactions, and SOCE. The IRE1-STIM1 axis regulates Ca^{2+} homeostasis, promoting T cell activation and human myoblast differentiation, and is activated during ER stress to sustain proteostasis. Using a genome-wide screen with the Ca^{2+} biosensor CaMPARI2,²⁴ we further identify the calmodulin kinase *CAMKG2* and the glutamine carrier *slc105a* as positive modulators of SOCE during ER stress. Our findings uncover an IRE1-STIM1 axis linking the UPR and SOCE to integrate two major functions of the ER, proteostasis and Ca^{2+} storage, with implications for immune and muscle physiology.

RESULTS

IRE1 promotes STIM1-mediated ER/PM tethering and SOCE

We and other authors have reported a major role for IRE1 protein on cellular Ca^{2+} homeostasis, either via ITPR (ITPR/IP₃R)^{21,22} or via ryanodine receptors (RyRs),^{25,26} both central components of the ER Ca^{2+} signaling machinery. To further unveil potential regulation of IRE1 on ER Ca^{2+} machinery, we used IRE1-deficient mouse embryonic fibroblasts (MEFs), where we stably re-expressed an empty vector or hemagglutinin (HA)-tagged IRE1 (IRE1-HA), a strategy that restored IRE1 expression and UPR to endogenous levels (Figures S1A and S1B). In these lines, we first validated with Fura-2 the Ca^{2+} responses of ITPR/IP₃R using a phospholipase C (PLC) chemical activator, M3M3FBS,²⁷ in calcium-free extracellular media (Figure S1C). Ca^{2+} responses of higher amplitude were observed in cells reconstituted with IRE1 as previously reported.²² We then performed a proteomic analysis on MEF cells knockout for IRE1 compared to stably re-expressing ones, aiming to identify potential changes in proteins related to ER calcium homeostasis. LC/MS analysis of all the proteomes identified 7,327 proteins from 115,609 peptides, of which 121 were significantly regulated by IRE1 presence (Figures 1A and 1B; Table S1). Pathway enrichment analysis of these hits revealed alterations on cellular responses to stress, organelle organization, cytoskeleton organization, and apoptotic processes, among others (Figure S1D). Out of the 121 hits, 71 were downregulated and 50 were enhanced in IRE1-KO (knockout) compared to IRE1-HA cells. The latter group contained two key regulators of ER calcium homeostasis: ITPR1/IP₃R1, validating our earlier findings,²² and STIM1. Western blots confirmed a 1.5-fold increase in STIM1 levels in IRE1-KO cells (Figure 1C). IP₃R opening causes ER Ca^{2+} depletion, activating the SOCE pathway by promoting STIM1-mediated ORAI1 gating at the PM. We therefore tested if SOCE activation following activation of IP₃R or passive ER Ca^{2+} depletion using Tg was altered by IRE1 deficiency. M3M3FBS evoked larger and persistent Ca^{2+} responses in IRE1-HA cells, consistent with an increased entry of Ca^{2+} from the extracellular space (Figure S1E). We then directly measured SOCE by applying the SERCA blocker Tg to empty ER stores. Both the slope and amplitude of the Ca^{2+} response evoked by Ca^{2+} re-admission to Tg-treated cells were increased in cells re-expressing IRE1-HA, indicating that IRE1 promotes SOCE independently of ITPR (Figure 1D). An enhanced Ca^{2+} response was also evoked by Tg in IRE1-HA cells in Ca^{2+} -rich medium (Figure S1F). Basal SOCE, measured with the Mn²⁺ quenching assay, was also enhanced in IRE1-HA cells (Figure S1G). SOCE reflects the gating of ORAI1 channels by STIM1 at ER-PM MCSs. To assess whether the formation of ER-PM contacts was impacted by IRE1, we measured the PM recruitment of the ER marker GFP-KDEL by total internal reflection fluorescence (TIRF) microscopy. The GFP-KDEL intensity increased in the TIRF plane following Tg addition, reaching levels significantly higher in IRE1-reconstituted cells compared to KO cells (Figure S1H). We then co-expressed tagged IRE1 or STIM1 in cells lacking both the STIM1 and STIM2 isoforms (double KOs [DKOs]). No Tg-induced increase in TIRF

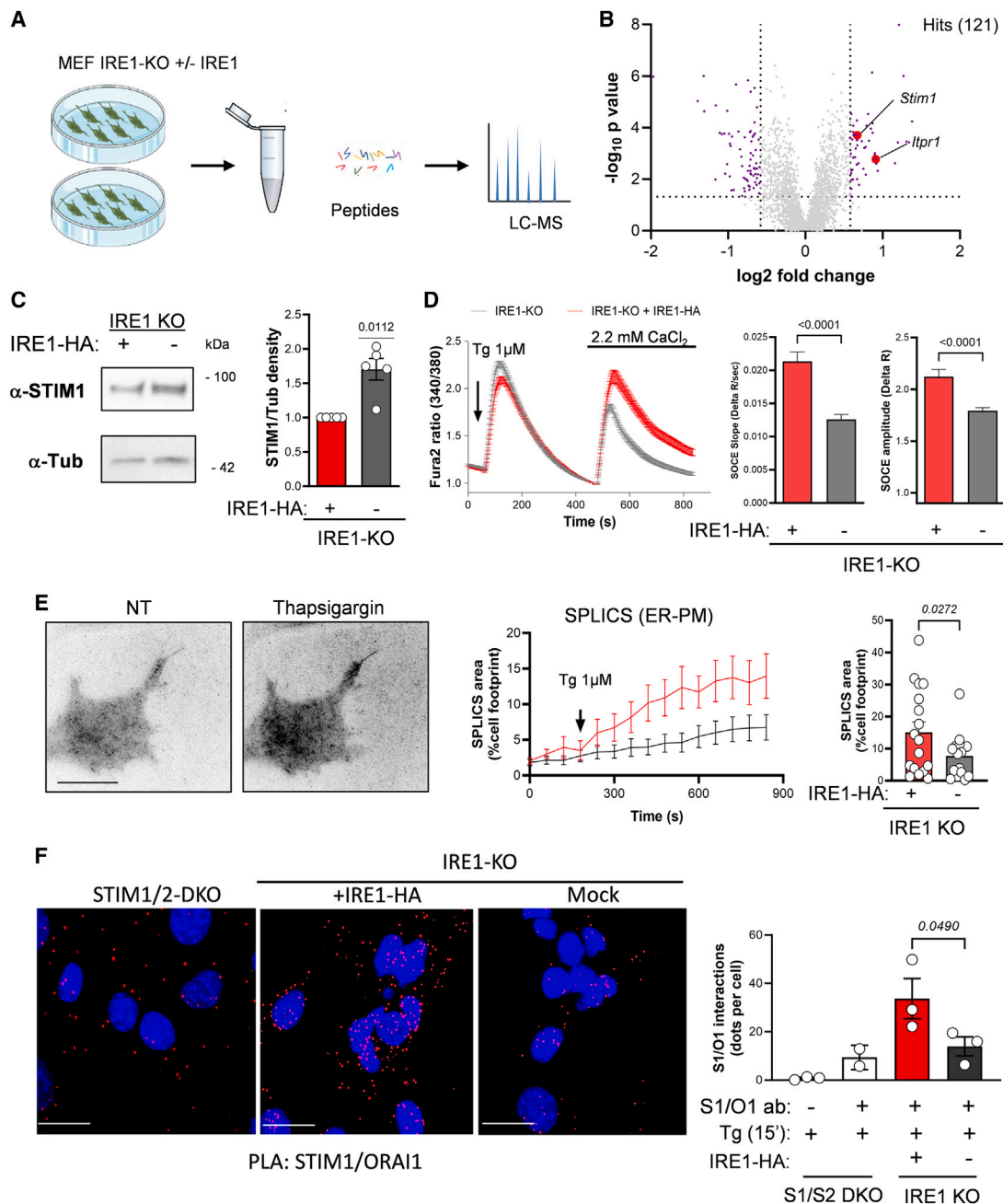


Figure 1. IRE1 α enhances SOCE by promoting STIM1-Orai1 interactions at ER-PM contact sites

(A) LC/MS workflow. MEF cells knocked out for IRE1 α (IRE1-KO) were generated and IRE1 α -HA re-expressed to endogenous levels to generate IRE1-HA cells. (B) Volcano plot showing the relative abundance of the proteins identified by LC/MS in IRE1-KO and IRE1-HA cells. Hits ($p > 0.05$ and fold change > 0.4) are highlighted in violet and STIM1 and ITPR1 in red.

(C) Western blot (WB) of IRE1-KO and IRE1-HA cells (left) and quantification of the STIM1 vs. tubulin immunoreactivities (mean \pm SEM, right, $n = 5$ independent experiments).

(D) Fura-2 responses evoked by Tg/ Ca^{2+} re-admission to IRE1-KO and IRE1-HA cells (mean \pm SEM, left) and averaged slope and amplitude of the SOCE responses (mean \pm SEM, right, $n = 220$ IRE1-KO and 198 IRE1-HA cells in 5 independent experiments).

(E) Fluorescence of ER-PM SPLICS in the TIRF plane before and after Tg addition to IRE1-KO and IRE1-HA cells (left), time course of the changes in SPLICS area in IRE1-KO and IRE1-HA cells (middle, mean \pm SEM), and fraction of the cell footprint covered by SPLICS in these cells at 800 s ($n = 17/16$ cells in 3 independent experiments, scale bar: 20 μ m).

(F) STIM1/Orai1 interactions reported by a protein ligation assay in STIM1/2 DKO, IRE1-KO, and IRE1-HA cells (left, red dots on the confocal micrographs, nuclei stained blue with DAPI, scale bar: 25 μ m) and quantification of the interactions (mean \pm SEM, right, $n = 3$ independent experiments).

Unpaired Student's t test (one tail on E and F).

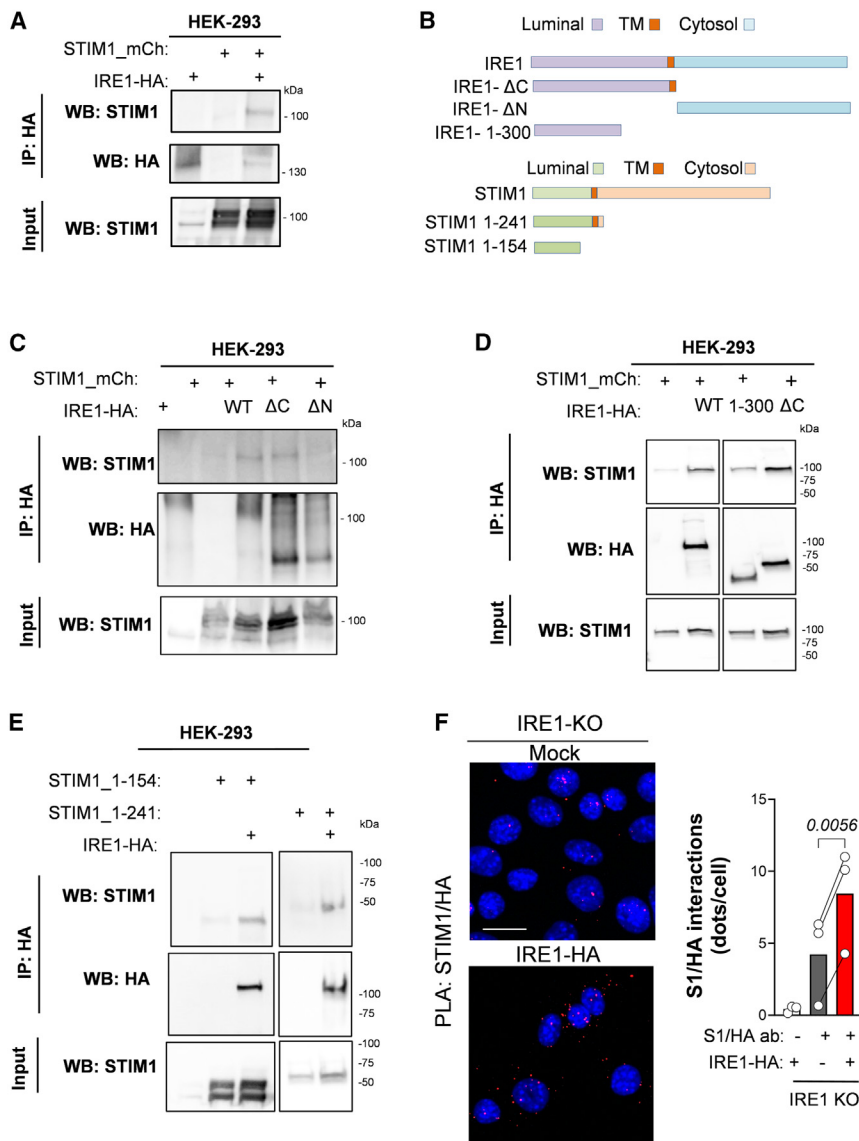


Figure 2. IRE1 α and STIM1 interact via their luminal domains

(A) Schematic topology of STIM1 and IRE1 truncation mutants used for immunoprecipitation (IP) studies (TM, transmembrane domain).

(B–E) STIM1 and HA immunoreactivities in lysates of HEK-293T cells transiently transfected with the indicated constructs and IPed with anti-HA antibodies. $n = 8$ (full-length), 5 (ΔC), and 3 (all other constructs) independent experiments.

(F) STIM1/IRE1 interactions reported by protein ligation assay (PLA) in IRE1-KO and IRE1-HA cells (left, red dots on the confocal micrographs, nuclei stained blue with DAPI, scale bar: 25 μm) and quantification of the interactions (right, $n = 3$ independent experiments, paired Student's t test).

IRE1 and STIM1 interact in the ER lumen

We next assessed whether IRE1 physically interacts with STIM1 to promote its translocation to the PM. IRE1 and STIM1 co-immunoprecipitated when overexpressed in HEK-293 cells (Figure 2A). To map the interacting domains within IRE1 and STIM1 we co-expressed STIM1-mCherry tagged (m-Ch) with truncated IRE1 mutants lacking the luminal domain (IRE1- ΔN) or the cytosolic domain (IRE1- ΔC) or retaining only IRE1's first 300 amino acids (IRE1 1–300). In parallel experiments, we co-expressed full-length IRE1-HA with truncated STIM1 mutants lacking the cytosolic domain (STIM1 1–241) or retaining only the first luminal 154 amino acids (STIM1 1–154) (Figure 2B). Co-immunoprecipitation (coIP) experiments revealed that the binding interphase of IRE1 is in the first 300 amino acids of the ER lumen (Figures 2C, 2D, and S2A). The interaction persisted when IRE1's full length was co-

expressed with STIM1 1–241 or the 1–154 mutant (Figures 2E and S2B). We then tested whether the monomeric or multimeric form of IRE1 promoted STIM1 function using cell lines stably expressing the IRE1-D123P mutant, which does not dimerize,²⁹ and observed that this potentiation relied on IRE1's monomeric form (Figure S2C). An interaction between endogenous STIM1 and re-expressed IRE1 was detected by PLA using IRE1-KO as control (Figure 2F). This interaction was reduced in cells exposed to Tg for 4 h but not in cells treated with tunicamycin (Tun) or Tg for 24 h (Figure S2D). These results establish that IRE1 promotes SOCE as a monomer via a complex with STIM1 on their luminal domains. This interaction decreases during acute exposure to Tg but not during ER stress induced by Tun.

fluorescence was observed in DKO cells when IRE1-GFP and mCh-KDEL were co-expressed, while both IRE1-GFP and GFP-KDEL efficiently accumulated in the TIRF plane when co-expressed with mCherry (mCh)-STIM1 (Figure S1I), indicating that the accumulation of these two ER proteins in cortical structures is mediated by STIM1. To more directly measure the formation of ER-PM MCSs, we used a split-GFP-based contact site sensor (SPLICS_L), which becomes fluorescent upon ER-PM contact site formation (Figure S1J).²⁸ SPLICS fluorescence in the TIRF plane increased following Tg-mediated store depletion, generating a significantly larger fluorescence footprint in IRE1-reconstituted cells (Figure 1E). Finally, a protein ligation assay (PLA) further indicated that the interactions between endogenous STIM1 and ORAI1 induced by Tg were enhanced by IRE1 re-expression (Figure 1F). These results indicate that IRE1 promotes the formation of STIM1-mediated ER-PM contact sites, enhancing STIM1-ORAI1 interactions and SOCE.

IRE1 deficiency impairs T cell activation

In T cells, SOCE activates the Ca²⁺-dependent phosphatase calcineurin, which dephosphorylates the nuclear factor of activated

T cells (NFAT), allowing its nuclear translocation to promote interleukin-2 (IL-2) cytokine expression.³⁰ To determine the physiological impact of the IRE1-STIM1 axis, we measured the nuclear translocation of a NFATc1-GFP construct in MEF cells deficient in or re-expressing IRE1 following Tg addition (Figure S3A). The time-dependent increase in nuclear GFP fluorescence as well as the GFP immunoreactivity of isolated nuclei were significantly higher in IRE1-HA reconstituted cells, indicating that IRE1 promotes NFATc1 translocation to the nucleus (Figures S3A and S3B). To assess the impact of the IRE1-STIM1 axis in T cells, we generated CRISPR-Cas9-mediated IRE1-KO and control Jurkat cells. Four KO clones were validated as devoid of IRE1 on western blots and lacking XBP1 splicing activity, with comparable mRNA levels of C/EBP homologous protein (*CHOP*) and *GRP94*/endoplasmic protein upon ER stress (Figures 3A, 3B, S3C, and S3D). Similarly to MEF cells, we observed an enhanced STIM1 expression in all four IRE1-KO clones (Figure 3B). Despite this compensation, SOCE recorded with Fluo8 and flow cytometry³¹ revealed that SOCE was slightly reduced in the IRE1-KO clones (Figure 3C). Accordingly, the levels of IL-2 transcript following activation by Tg were significantly reduced (Figure 3D). To translate these findings *in vivo*, we used transgenic mice carrying alleles enabling CD4-driven, T cell-specific IRE1 ablation ($CD4^{cre};IRE1\alpha^{fl/fl}$, Figure 3E).³² CD4 T cells isolated from $CD4^{cre};IRE1\alpha^{fl/fl}$ (KO) mice lacked IRE1 in western blots and failed to cleave XBP1 when treated with Tg (Figure 3F), validating the genetic ablation. Analysis of IL-2 mRNA levels revealed that IRE1 ablation prevented IL-2 induction even at Tg doses that did not trigger XBP1 splicing (Figure 3G). We then plated CD4 cells on coverslips coated with CD3/CD28 antibodies to activate the T cell receptor (TCR). In this setting, IRE1 ablation only marginally reduced CD3/CD28-mediated T cell activation (Figure S3E). These results indicate that IRE1 promotes T cell signaling by enhancing SOCE and potentiates effector responses triggered by Tg but not by TCR-mediated activation.

IRE1 promotes the differentiation of human myoblasts

In muscle, SOCE is required for myoblast differentiation and sustains ER refilling after repetitive exercise.³³ To assess the impact of IRE1 in this context, we collected muscular biopsies from human healthy donors and used CRISPR constructs targeting IRE1, validated in HEK-293 cells (Figure S4A). CRISPR editing reduced IRE1 expression by ~50% in human myoblasts (Figure 4A) and significantly decreased SOCE (Figure 4B) as well as the STIM1/ORAI1 interactions detected with PLA (Figure 4C). This same technique could verify that STIM1 and IRE1 interact either at endogenous levels (Figure 4D) or when IRE1-HA was re-expressed in IRE1-KO myoblasts (Figure S4B). This latter strategy also rescued STIM1 and ORAI1 interactions (Figure S4C). To evaluate the effects of IRE1 on muscle differentiation, we quantified the levels of two differentiation markers, myocyte enhancer factor 2C (MEF2C) and myosin heavy chain (MyHC), expressed once myoblasts fuse into myotubes.³³ The expression levels of MEF2C and MyHC were decreased in IRE1-depleted myoblasts cultured for 48 and 72 h in medium promoting differentiation, indicating that IRE1 deficiency delays myoblast differentiation into myotubes (Figures 4E–4G). These

data indicate that IRE1 interacts with STIM1, enhances SOCE, and promotes the differentiation of myoblasts into myotubes.

STIM1 promotes IRE1 activity

Our results indicate that IRE1 promotes STIM1 activity and gating of ORAI1 in immune and muscle cells. To investigate whether STIM1, in turn, impinges on IRE1 activation by ER stress, we transduced primary human myoblasts with a doxycycline-inducible microRNA (miRNA) targeted to STIM1, a procedure that reduced STIM1 levels and SOCE by >50% (Figures 4H and 4I). We then treated these cells with Tun or Tg to study Ca^{2+} -dependent and -independent ER stress in the presence or absence of STIM1. We evaluated *GRP94*, *CHOP*, and *XBP1s* mRNA induction as readouts for ATF6, PERK, and IRE1 signaling, respectively (Figure S4D). STIM1 depletion decreased basal mRNA levels of *XBP1s* but not of *GRP94* or *CHOP* (Figures 4J and S4F–S4H), indicating that basal ER stress levels rely on STIM1. Accordingly, the UPRE activity measured with a luciferase assay was increased by re-expressing STIM1 in STIM1/2 DKO cells (Figure S4J). Addition of Tg increased *XBP1s* levels severalfold at 4 and 24 h, an ER stress response that was significantly diminished by STIM1 depletion in myoblasts (Figure 4J). Correspondingly, the UPRE response induced by Tg was augmented by STIM1 re-expression in DKO MEFs (Figure S4E). In contrast, neither the *XBP1s* increase evoked by Tun nor the ATF6 and PERK pathways evoked by Tg or Tun were impacted by changes in STIM1 expression (Figures S4D–S4I). These results suggest that STIM1 is required for IRE1 signaling triggered by ER Ca^{2+} stores depletion.

CaMP screen identifies SOCE modulators under ER stress

The preserved IRE1-STIM1 interactions in cells treated with Tun (Figure S2D) suggested that the IRE1-STIM1 axis is functional during the ER stress response induced by the inhibition of protein glycosylation. Accordingly, acute (4 h) Tun treatment potentiated SOCE in cells re-expressing IRE1 but did not impact SOCE in IRE1-KO cells (Figures S5A and S5B). To identify the molecular basis of this potentiation, we performed a whole-genome genetic screen using a Ca^{2+} -modulated photoactivatable ratiometric integrator (CaMPARI) as bioreporter, which irreversibly photoconverts from green to red upon UV light excitation only at Ca^{2+} concentrations exceeding 200 nM.³⁴ The procedure was validated with cells lacking ORAI isoforms (Figure S5C) and with the CaMPARI2²⁴ (CaMP2) probe stably expressed in MEF cells deficient in or re-expressing IRE1 (Figure S5D). UV illumination during exposure to Tg resulted in effective photoconversion (Figure 5A), while the reversible SERCA blocker cyclopiazonic acid (CPA) used at nontoxic doses (Figure S5E) enabled the detection by flow cytometry of cells with high SOCE, whose proportion was enriched in cells reconstituted with IRE1 (Figures 5B and S5F). Tun further increased the fraction of photoconverted cells but only when IRE1 was re-expressed (Figure 5C). To identify genes mediating SOCE potentiation downstream of IRE1, Cas9 and a whole mouse genome single guide RNA (sgRNA) library (4 sgRNAs per gene, Brie library³⁵) were integrated in cells expressing IRE1 and CaMP2. The cells were then photoconverted during CPA-mediated SOCE and sorted in a flow

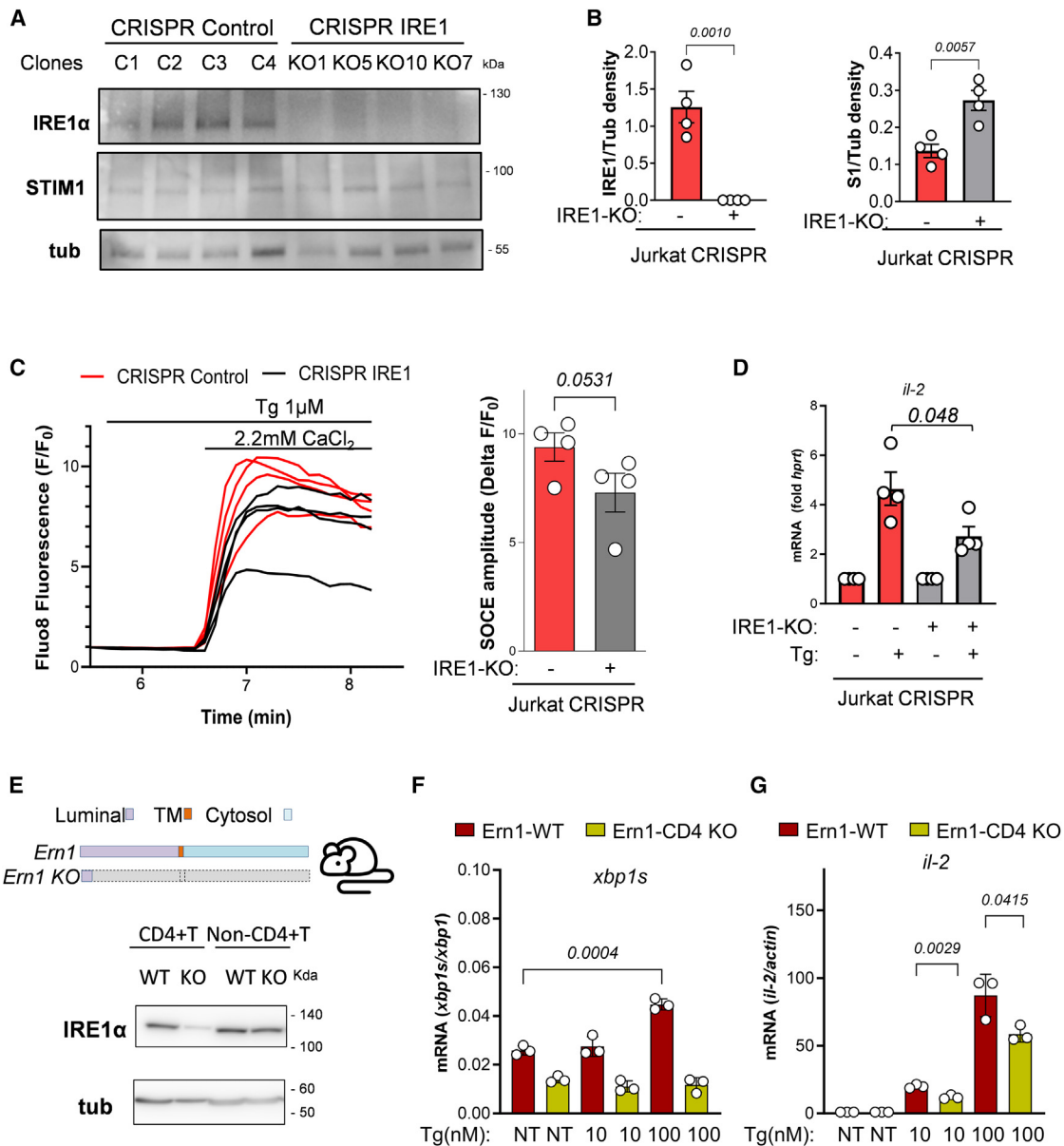


Figure 3. IRE1 α ablation prevents store-dependent T cell activation

(A) WB of Jurkat T cells lines generated by CRISPR with control or IRE1-targeted sequences.

(B) Quantification of STIM1 and IRE1 expression levels in these lines (mean \pm SEM).

(C) Flow cytometry Fluo-8 recordings of control and IRE1-CRISPR Jurkat T cells during Tg/Ca²⁺ re-admission (left) and quantification of the SOCE responses (right). Each line/dot shows the mean value from 2–3 independent experiments for each clone. Graph bars represent mean \pm SEM from clones.

(D) Interleukin-2 (IL-2) mRNA levels of control and IRE1-KO Jurkat T cells exposed or not to 100 nM Tg for 6 h. Data are mean values \pm SEM from 2 independent experiments for each clone.

(E) WB of primary T cells from WT and Ern1-CD4 CRE mouse.

(F and G) *xbp1s* and *il-2* mRNA levels of Ern1 WT and KO T cells exposed to 10 or 100 nM Tg for 6 h. Data are mean \pm SEM of 3 mice per group.

Unpaired Student's t test one (C) or two tailed (D, F, and G).

citometer for a low (<10%) photoconversion rate (Figure 5D). Next-generation sequencing and genome enrichment analyses identified 4,012 sgRNAs (5% of total) that reduced SOCE, including STIM1 and Orai1, which ranked with maximal significance, validating the screen (Figures 5E and S5G). We then selected genes targeted by 2 or more sgRNAs enriched in cells

treated with Tun and retaining a low SOCE. This strategy identified 5 genes whose disruption prevented the SOCE potentiation associated with this specific ER stress condition (Figure 5F; Tables S2 and S3). Among these were calcium/calmodulin-dependent protein kinase II gamma (CAMK2G), involved in apoptosis mediated by FAS under ER stress³⁶ and muscular

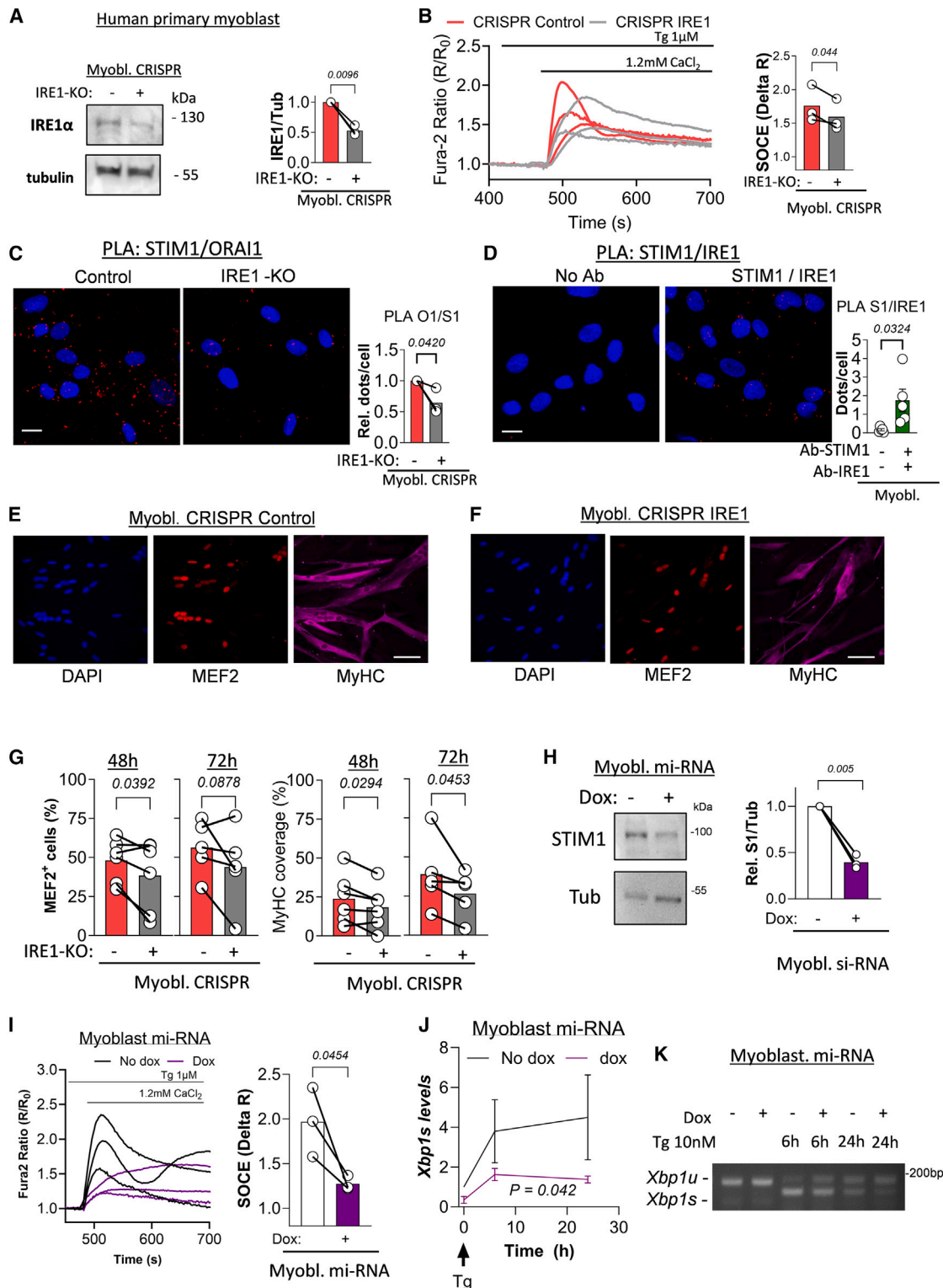


Figure 4. IRE1 promotes SOCE and myoblast differentiation

(A) WB of human primary myoblasts generated by CRISPR with control or IRE1-targeted sequences (left) and quantification of IRE1 protein levels in these cells populations (right, n = 3 independent experiments).

(B) Mean fura-2 responses for every donor evoked by Tg/Ca²⁺ re-admission to control and IRE1-CRISPR myoblasts (left) and quantification of the SOCE amplitude (right, n = 3 donors with >35 cells each in duplicate, data paired by donor).

(legend continued on next page)

activity,³⁷ and the glutamine carrier protein SLC1A5 involved in cancer, ER stress, and T cell function.^{38,39} Inhibition of CAMK2G by KN-62 and of SLC1A5 by L-glutamic acid γ -(p-nitroanilide) (GPNA) prevented the potentiation of SOCE by Tun (Figures 5G and S5H–S5J), validating these two hits. These data show that a CAMPARI screen can identify genes coding for critical genes and modulators of cellular Ca^{2+} fluxes, enabling us to identify two proteins that promote SOCE specifically during acute ER stress.

DISCUSSION

ER stress signaling and SOCE have been studied as separate processes for several years despite their common reliance on ER calcium homeostasis. Reductions in ER Ca^{2+} levels sensed by STIM proteins trigger SOCE to refill ER stores, while UPR transducers sense the same Ca^{2+} drop to trigger a signaling pathway aiming to restore ER homeostasis. For this reason, SERCA blockers commonly used to trigger and measure SOCE activity are frequently used to trigger ER stress.⁴⁰ Several studies have identified positive and negative modulators of UPR members, including proteins regulating post-translational modifications that impact IRE1 activity and stability (reviewed in Urrea et al.⁴¹). This “UPRosome” forms a network of proteins that on one hand fine-tune IRE1 signaling and on the other confer functions to IRE1 in controlling actin dynamics and ER-mitochondria Ca^{2+} transfer.^{22,23} A role for IRE1 in Ca^{2+} homeostasis was also proposed based on the close apposition between IRE1 and RyRs in muscle.^{26,42} Here, we uncover the link between IRE1 and calcium homeostasis by proteomic analysis and show that ITPR1 and STIM1 are upregulated in IRE1-deficient cells, a phenomenon most likely compensating for an altered ER Ca^{2+} homeostasis. Since we already documented the interactions between IRE1 and ITPRs, we focused on STIM1. We show that IRE1 forms a complex with STIM1 in the ER lumen and promotes the generation of MCSs, ORAI1 trapping by STIM1, and SOCE. We show that IRE1 interacts with STIM1 in the ER lumen, either directly or via common interactors⁴³ like ITPRs or chaperones like GRP78 (Hspa5) or SigmaR1.⁴⁴ STIM1 undergoes complex conformational changes during activation,⁴⁵ and whether IRE1 impacts specific activation steps during STIM1 translocation to ER-PM junctions via a direct interaction or via protein complexes remains to be explored.

We also establish the functional impact of IRE1 ablation on SOCE and downstream signaling in primary mouse T cells and human myoblasts, thereby highlighting the physiological role of

the IRE1-STIM1 axis. Our findings are of clinical relevance because loss-of-function mutations in human STIM1 or ORAI1 cause defective T cell activation and severe combined immunodeficiency (SCID).⁴⁶ Of note, IRE1 has also been linked to immune system development and differentiation⁴⁷ and can act as T cell suppressor when activated by the tumor microenvironment.⁴⁸ In human muscle, on the other hand, gain-of-function mutations in STIM1 and ORAI1 lead to tubular aggregate myopathies, which exhibit a strong component of ER stress.⁴⁹ IRE1 activity promotes muscular regeneration after injury,⁵⁰ and calsequestrin, an ER chaperone genetically linked to TAM,⁵¹ binds to IRE1 in muscular systems.⁴² This evidence highlights the relevance of the crosstalk that we uncover here between IRE1 and STIM1 for human pathologies.

The clear reliance of STIM1 on IRE1 in human primary myoblasts prompted us to evaluate the bidirectionality of this pathway by testing whether STIM1 levels modulate UPR induction in muscle. Our results show that the PERK and ATF6 axis does not rely on STIM1, while IRE1 signaling depends on STIM1 for ER stress triggered by Ca^{2+} depletion but not for ER stress triggered by inhibition of N-glycosylation. This suggests that IRE1 and STIM1 cooperatively respond to alterations in ER Ca^{2+} homeostasis. In mouse skeletal or cardiac muscle, STIM1 depletion enhanced ER stress and proteostasis defects,^{52,53} an effect opposite to the one that we report here, while in human goblet cells, STIM1 depletion reduced ER stress, suggesting that the outcome of the IRE1-STIM1 crosstalk might be tissue and context specific.⁵⁴

Our observations that SOCE is boosted under acute ER stress were also previously reported in pancreatic cells, where low-Tun treatments enhanced calcium oscillations.⁵⁵ Since SOCE is critical for T cell activation,⁵⁶ and since the tumor microenvironment (TME) promotes T cell immunosuppression via ER stress,^{57,58} we aimed to explore those proteins involved in SOCE boosting. We identified several modulators and validated the calmodulin kinase CAMK2, linked to cell death under ER stress,³⁶ and the glutamine carrier SLC1A5, related to ER stress and cancer,^{38,39} as positive SOCE modulators during ER stress. Further studies should aim to determine how those proteins are regulated by IRE1 during ER stress and whether they can be exploited in context of immune suppression or overactivation.

In summary, we describe IRE1 as a steady-state housekeeper of ER Ca^{2+} homeostasis via SOCE and establish that STIM1 is needed for a proper IRE1 activation. Our screening using CaMPARI2 identified CAMK2 and SLC1A5 as proteins that potentiate SOCE during ER stress. We propose that IRE1

(C) STIM1/Orai1 interactions reported by PLA in control and IRE1-CRISPR myoblasts treated with Tg for 15 min (left, scale bar: 20 μm) and quantification of the interactions (right, $n = 3$ donors with >40 cells each).

(D) STIM1/IRE1 PLA in human primary myoblasts (left) and quantification of the interactions (right, $n = 5$ independent scorings in 3 donors with >200 cells each).

(E and F) Micrographs of MEF2C and MyHC immunostaining in control and IRE1-CRISPR myoblasts differentiated for 72 h (scale bar: 20 μm).

(G) Fraction of cells positive for MEF2C (left) and MyHC (right) after 48 and 72 h differentiation ($n = 6$ and 5 donors, respectively, with 5 fields analyzed per donor).

(H) WB of human primary myoblasts transduced with a doxycycline-inducible STIM1 miRNA (Myobl. miRNA) treated or not with 1 μM doxycycline for 72 h (left) and quantification of STIM1 protein levels in these two cells populations (right, $n = 3$ donors).

(I) Mean fura-2 responses for every donor evoked by Tg/ Ca^{2+} re-admission to control and STIM1-depleted myoblasts (left) and quantification of the SOCE amplitude (right, $n = 3$ donors with >30 cells each in two separate recordings).

(J and K) XBP1s splicing assayed by qPCR (mean \pm SEM, J) or gel electrophoresis (K) in control and STIM1-depleted myoblasts stimulated with Tg 10 nM for 6 and 24 h ($n = 3$ donors).

Statistical analyses were performed with paired Student's t test (one tail) except for (J), where a two-way ANOVA was applied.

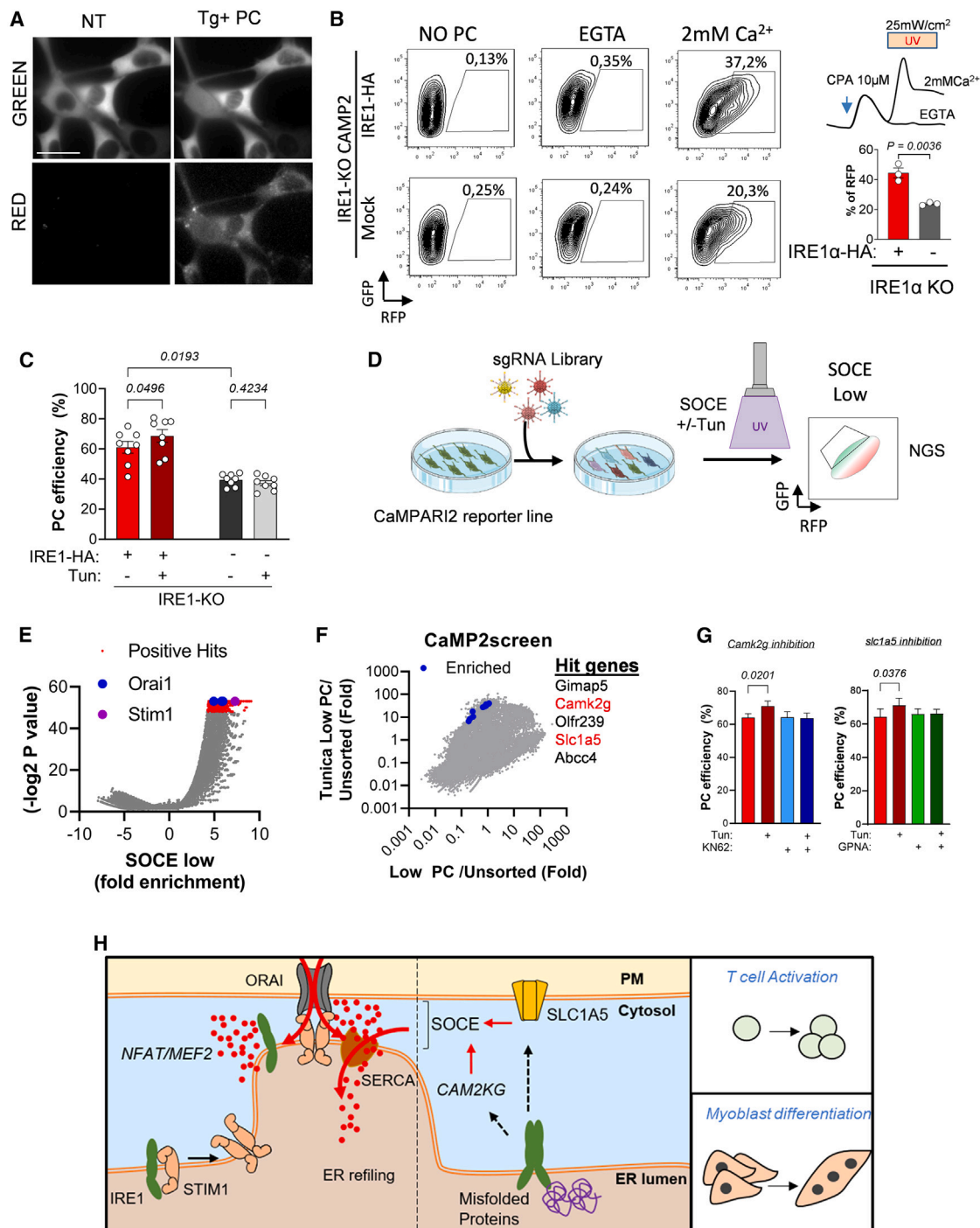


Figure 5. CaMPARI2 screening identifies SOCE modulators downstream of IRE1 α

(A) Micrographs of MEF cells stably expressing CaMPARI2, exposed or not to 1 μ M Tg/Ca²⁺ and UV light for photoconversion (PC). The photoconverted CaMPARI2 appears in the red channel (bottom, scale bar: 50 μ m).

(B) Flow cytometry profiles of IRE1-KO and IRE1-HA cells treated with CPA and photoconverted in Ca²⁺-free (EGTA) or Ca²⁺-rich (2 mM Ca²⁺) media (top right, protocol) and mean \pm SEM fraction of RFP-positive cells (bottom right, n = 3 independent experiments, unpaired Student's t test).

(C) Effect of Tun (Tun, 200 ng/mL for 4 h) on PC efficiency during Tg/Ca²⁺ re-admission to IRE1-KO and IRE1-HA cells (mean \pm SEM % of PC positive cells, n = 8 measurements in 3 independent experiments, ANOVA with Šídák's multiple comparisons test).

(D) Scheme of the CaMPARI2 screening strategy.

(E) Volcano plot showing the relative abundance of sgRNAs in cells exhibiting a low PC efficiency (SOCE low). Significant hits are highlighted in red and Orai1 and STIM1 sgRNAs in blue and violet.

(legend continued on next page)

regulates ER Ca²⁺ homeostasis by interacting with STIM1 to sustain ER Ca²⁺ levels and thus proteostasis, an interaction potentiated under ER stress by CAMKG2 and SLC1A5 (Figure 5H). Targeting this axis might have therapeutic value in pathologies associated with ER Ca²⁺ dysregulations such as cancer, immune dysregulation, neurodegeneration, or aging.^{49,59}

Limitations of the study

Our findings that IRE1 and STIM1 interact to sustain each other's activity in human myoblasts and Jurkat T cells contrasts with earlier reports linking STIM1 deficiency to enhanced ER stress and proteostasis defects in mouse skeletal or cardiac muscle.^{52,53} In our hands, STIM1 silencing reduced IRE1 function only when ER stress was induced by ER Ca²⁺ store depletion. We acknowledge that these discrepancies might reflect differences between *in vivo* and *ex vivo* models, interspecies differences (mouse vs. human), and/or KO vs. silencing strategies. We also acknowledge that documenting the interactions between proteins overexpressed in HEK-293 cells required high exposures on western blots (see uncut gels), suggesting that the interaction might be weak or indirect. Another limitation is that we cannot discard that the interaction between the two proteins in the ER lumen is bridged by other known STIM1 and/or IRE1 interactors like ITPRs or chaperones like GRP78 (Hspa5) or SigmaR1.⁴⁴

STAR★METHODS

Detailed methods are provided in the online version of this paper and include the following:

- KEY RESOURCES TABLE
- RESOURCE AVAILABILITY
 - Lead contact
 - Materials availability
 - Data and code availability
- EXPERIMENTAL MODEL AND STUDY PARTICIPANT DETAILS
 - Human primary myoblasts
 - ERN1 CD4 cre studies
- METHOD DETAILS
 - Antibodies and reagents
 - Cell culture and stable cell lines
 - Western blot analysis
 - Immunofluorescence, protein ligation assays and TIRF
 - Immunoprecipitation
 - Calcium measurements using FURA2, Fluo4 and FDSS
 - Luciferase measurements
 - CAMPARI calcium measurements
 - CAMPARI2 CRISPR screening
 - RNA isolation, PCR and qPCR
 - NFAT translocation assays

○ LC/MS studies

● QUANTIFICATION AND STATISTICAL ANALYSIS

SUPPLEMENTAL INFORMATION

Supplemental information can be found online at <https://doi.org/10.1016/j.celrep.2023.113540>.

ACKNOWLEDGMENTS

We thank Dr. Laumonier and all the members of the Frieden group for their help and assistance and Dr. M. Bachman for feedback in this project and for sharing reagents. We also thank Dr. Ling Qi for providing IRE1 α mutant constructs, Dr. Tito Cali for the SPLICS ER/mitochondria constructs, David Ron for providing IRE1 α -null MEFs, and Anjana Rao for providing the DKO STIM1/2 cells. We also thank all members of the Demarex lab for their insightful discussions and the Bioimaging, READS, Proteomics, Genomics, and Flow Cytometry platforms/facilities (Geneva Medical Center). This work was funded by the Sir Jules Thorn Foundation (2022), the FSRMM, and the Novartis Young investigation Grant (22B082) (A.C.-S.); the US Air Force Office of Scientific Research FA9550-21-1-0096, FONDAP program 15150012, Department of Defense grant W81XWH2110960, ANID/FONDEF ID1D22110120, and ANID/NAM2210057 (C.H.); and the Swiss National Foundation (grant numbers 310030_184756 [to M.F.] and 310030_189042 [to N.D.]).

AUTHOR CONTRIBUTIONS

A.C.-S. and N.D. designed the study. A.C.-S., X.Z., L.L., J.B., X.W., and C.C. performed experiments and analyzed the data. C.H., Y.L., M.F., N.D., and A.C.-S. supervised experiments and participated in the design. A.C.-S. wrote the manuscript. N.D. edited the manuscript. All authors read and approved the final version of the manuscript.

DECLARATION OF INTERESTS

The authors declare no competing interests.

INCLUSION AND DIVERSITY

We support inclusive, diverse, and equitable conduct of research.

Received: June 5, 2023

Revised: September 29, 2023

Accepted: November 20, 2023

Published: December 5, 2023

REFERENCES

1. Walter, P., and Ron, D. (2011). The Unfolded Protein Response: From Stress Pathway to Homeostatic Regulation. *Science* 334, 1081–1086.
2. Kaufman, R.J. (1999). Stress signaling from the lumen of the endoplasmic reticulum: Coordination of gene transcriptional and translational controls. *Genes Dev.* 13, 1211–1233.
3. Tabas, I., and Ron, D. (2011). Integrating the mechanisms of apoptosis induced by endoplasmic reticulum stress. *Nat. Cell Biol.* 13, 184–190.
4. Hetz, C., Zhang, K., and Kaufman, R.J. (2020). Mechanisms, regulation and functions of the unfolded protein response. *Nat. Rev. Mol. Cell Biol.* 21, 421–438.

(F) Relative abundance of sgRNAs in cells treated or not with Tun and exhibiting a low PC efficiency. sgRNAs enriched >35-fold detected at least 2 times are highlighted in blue, and names of genes are indicated with validated hits highlighted in red.

(G) Effect of inhibitors of CAMKG2 (KN62, left) or SLC1A5 (GPNA, right) on PC efficiency during Tg/Ca²⁺ re-admission to IRE1-HA cells treated or not with Tun as in (C) (mean \pm SEM % of PC positive cells, n = 8 measurements in 3 independent experiments, unpaired Student's t test).

(H) Cartoon of the proposed model.

5. Hetz, C. (2021). Adapting the proteostasis capacity to sustain brain health-span. *Cell* 184, 1545–1560.
6. Prakriya, M., and Lewis, R.S. (2015). Store-operated calcium channels. *Physiol. Rev.* 95, 1383–1436.
7. Missiaen, L., Taylor, C.W., and Berridge, M.J. (1991). Spontaneous calcium release from inositol trisphosphate-sensitive calcium stores. *Nature* 352, 241–244.
8. Roos, J., DiGregorio, P.J., Yeromin, A.V., Ohlsen, K., Lioudyno, M., Zhang, S., Safrina, O., Kozak, J.A., Wagner, S.L., Cahalan, M.D., et al. (2005). STIM1, an essential and conserved component of store-operated Ca²⁺ channel function. *J. Cell Biol.* 169, 435–445.
9. Zhang, S.L., Yu, Y., Roos, J., Kozak, J.A., Deerinck, T.J., Ellisman, M.H., Stauderman, K.A., and Cahalan, M.D. (2005). STIM1 is a Ca²⁺ sensor that activates CRAC channels and migrates from the Ca²⁺ store to the plasma membrane. *Nature* 437, 902–905.
10. Liou, J., Kim, M.L., Heo, W.D., Jones, J.T., Myers, J.W., Ferrell, J.E., and Meyer, T. (2005). STIM Is a Ca²⁺ Sensor Essential for Ca²⁺-Store-Depletion-Triggered Ca²⁺ Influx. *Curr. Biol.* 15, 1235–1241.
11. Vig, M., Peinelt, C., Beck, A., Koomoa, D.L., Rabah, D., Koblan-Huberson, M., Kraft, S., Turner, H., Fleig, A., Penner, R., and Kinet, J.P. (2006). CRACM1 Is a Plasma Membrane Protein Essential for Store-Operated Ca²⁺ Entry. *Science* 312, 1220–1223.
12. Feske, S., Gwack, Y., Prakriya, M., Srikanth, S., Puppel, S.-H., Tanasa, B., Hogan, P.G., Lewis, R.S., Daly, M., and Rao, A. (2006). A mutation in Orai1 causes immune deficiency by abrogating CRAC channel function. *Nature* 441, 179–185.
13. Prakriya, M., Feske, S., Gwack, Y., Srikanth, S., Rao, A., and Hogan, P.G. (2006). Orai1 is an essential pore subunit of the CRAC channel. *Nature* 443, 230–233.
14. Feske, S. (2011). Immunodeficiency due to defects in store-operated calcium entry. *Ann. N. Y. Acad. Sci.* 1238, 74–90.
15. Kiviliuto, S., Decuypere, J.-P., De Smedt, H., Missiaen, L., Parys, J.B., and Bultynck, G. (2011). STIM1 as a key regulator for Ca²⁺ homeostasis in skeletal-muscle development and function. *Skeletal Muscle* 1, 16.
16. Wei-Lapierre, L., Carrell, E.M., Boncompagni, S., Protasi, F., and Dirksen, R.T. (2013). Orai1-dependent calcium entry promotes skeletal muscle growth and limits fatigue. *Nat. Commun.* 4, 2805.
17. Berridge, M.J., Lipp, P., and Bootman, M.D. (2000). The versatility and universality of calcium signalling. *Nat. Rev. Mol. Cell Biol.* 1, 11–21.
18. Manford, A.G., Stefan, C.J., Yuan, H.L., MacGurn, J.A., and Emr, S.D. (2012). ER-to-Plasma Membrane Tethering Proteins Regulate Cell Signaling and ER Morphology. *Dev. Cell* 23, 1129–1140.
19. van Vliet, A.R., Giordano, F., Gerlo, S., Segura, I., Van Eygen, S., Molenberghs, G., Rocha, S., Houcine, A., Derua, R., Verfaillie, T., et al. (2017). The ER Stress Sensor PERK Coordinates ER-Plasma Membrane Contact Site Formation through Interaction with Filamin-A and F-Actin Remodeling. *Mol. Cell* 65, 885–899.e6.
20. Hetz, C., and Papa, F.R. (2018). The Unfolded Protein Response and Cell Fate Control. *Mol. Cell* 69, 169–181.
21. Son, S.M., Byun, J., Roh, S.-E., Kim, S.J., and Mook-Jung, I. (2014). Reduced IRE1 α mediates apoptotic cell death by disrupting calcium homeostasis via the InsP3 receptor. *Cell Death Dis.* 5, e1188.
22. Carreras-Sureda, A., Jaña, F., Urra, H., Durand, S., Mortenson, D.E., Sagredo, A., Bustos, G., Hazari, Y., Ramos-Fernández, E., Sassano, M.L., et al. (2019). Non-canonical function of IRE1 α determines mitochondria-associated endoplasmic reticulum composition to control calcium transfer and bioenergetics. *Nat. Cell Biol.* 21, 755–767.
23. Urra, H., Henríquez, D.R., Cánovas, J., Villarroel-Campos, D., Carreras-Sureda, A., Pulgar, E., Molina, E., Hazari, Y.M., Limia, C.M., Alvarez-Rojas, S., et al. (2018). IRE1 α governs cytoskeleton remodelling and cell migration through a direct interaction with filamin A. *Nat. Cell Biol.* 20, 942–953.
24. Moeyaert, B., Holt, G., Madangopal, R., Perez-Alvarez, A., Fearey, B.C., Trojanowski, N.F., Ledderose, J., Zolnik, T.A., Das, A., Patel, D., et al. (2018). Improved methods for marking active neuron populations. *Nat. Commun.* 9, 4440.
25. Papaioannou, A., Centonze, F., Metais, A., Maurel, M., Negroni, L., Gonzalez-Quiroz, M., Mahdizadeh, S.J., Svensson, G., Zare, E., Blondel, A., et al. (2022). Stress-induced tyrosine phosphorylation of RtcB modulates IRE1 activity and signaling outputs. *Life Sci. Alliance* 5, e202201379.
26. Agellon, L.B., and Michalak, M. (2019). Avoiding raising the ire of IRE1 α . *Cell Calcium* 83, 102056.
27. Bae, Y.S., Lee, T.G., Park, J.C., Hur, J.H., Kim, Y., Heo, K., Kwak, J.Y., Suh, P.G., and Ryu, S.H. (2003). Identification of a compound that directly stimulates phospholipase C activity. *Mol. Pharmacol.* 63, 1043–1050.
28. Vallese, F., Catoni, C., Cieri, D., Barazzuol, L., Ramirez, O., Calore, V., Bonora, M., Giamogante, F., Pinton, P., Brini, M., and Cali, T. (2020). An expanded palette of improved SPLICS reporters detects multiple organelle contacts in vitro and in vivo. *Nat. Commun.* 11, 6069.
29. Xue, Z., He, Y., Ye, K., Gu, Z., Mao, Y., and Qi, L. (2011). A Conserved Structural Determinant Located at the Interdomain Region of Mammalian Inositol-requiring Enzyme 1 α . *J. Biol. Chem.* 286, 30859–30866.
30. Macian, F. (2005). NFAT proteins: key regulators of T-cell development and function. *Nat. Rev. Immunol.* 5, 472–484.
31. Carreras-Sureda, A., Abrami, L., Ji-Hee, K., Wang, W.-A., Henry, C., Frieden, M., Didier, M., van der Goot, F.G., and Demareux, N. (2021). S-acylation by ZDHHC20 targets ORAI1 channels to lipid rafts for efficient Ca²⁺ signaling by Jurkat T cell receptors at the immune synapse. *Elife* 10, e72051.
32. Shao, M., Shan, B., Liu, Y., Deng, Y., Yan, C., Wu, Y., Mao, T., Qiu, Y., Zhou, Y., Jiang, S., et al. (2014). Hepatic IRE1 α regulates fasting-induced metabolic adaptive programs through the XBP1s–PPAR α axis signalling. *Nat. Commun.* 5, 3528.
33. Darbellay, B., Arnaudeau, S., König, S., Jousset, H., Bader, C., Demareux, N., and Bernheim, L. (2009). STIM1- and Orai1-dependent Store-operated Calcium Entry Regulates Human Myoblast Differentiation. *J. Biol. Chem.* 284, 5370–5380.
34. Fosque, B.F., Sun, Y., Dana, H., Yang, C.T., Ohyama, T., Tadross, M.R., Patel, R., Zlatic, M., Kim, D.S., Ahrens, M.B., et al. (2015). Labeling of active neural circuits in vivo with designed calcium integrators. *Science* 347, 755–760.
35. Doench, J.G., Fusi, N., Sullender, M., Hegde, M., Vaimberg, E.W., Donovan, K.F., Smith, I., Tothova, Z., Wilen, C., Orchard, R., et al. (2016). Optimized sgRNA design to maximize activity and minimize off-target effects of CRISPR-Cas9. *Nat. Biotechnol.* 34, 184–191.
36. Timmins, J.M., Ozcan, L., Seimon, T.A., Li, G., Malagelada, C., Backs, J., Backs, T., Bassel-Duby, R., Olson, E.N., Anderson, M.E., and Tabas, I. (2009). Calcium/calmodulin-dependent protein kinase II links ER stress with Fas and mitochondrial apoptosis pathways. *J. Clin. Invest.* 119, 2925–2941.
37. Rose, A.J., Kiens, B., and Richter, E.A. (2006). Ca²⁺-calmodulin-dependent protein kinase expression and signalling in skeletal muscle during exercise. *J. Physiol.* 574, 889–903.
38. Jeon, Y.J., Khelifa, S., Ratnikov, B., Scott, D.A., Feng, Y., Parisi, F., Ruller, C., Lau, E., Kim, H., Brill, L.M., et al. (2015). Regulation of Glutamine Carrier Proteins by RNF5 Determines Breast Cancer Response to ER Stress-Inducing Chemotherapies. *Cancer Cell* 27, 354–369.
39. Wang, W., Guo, M., Bai, Z., Bai, W., Chen, W., Su, Y., and Wu, J. (2022). Dysfunction of Cytotoxic T Lymphocyte Induced by Hepatoma Cells through the Gln-GLS2-Endoplasmic Reticulum Stress Pathway. *Front. Biosci.* 27, 243.
40. Carreras-Sureda, A., Pihán, P., and Hetz, C. (2017). Calcium signaling at the endoplasmic reticulum: Fine-tuning stress responses. *Cell Calcium* 70, 24–31.
41. Urra, H., Pihán, P., and Hetz, C. (2020). The UPProsome – decoding novel biological outputs of IRE1 α function. *J. Cell Sci.* 133, jcs218107.

42. Wang, Q., Groenendyk, J., Paskevicius, T., Qin, W., Kor, K.C., Liu, Y., Hies, F., Knollmann, B.C., Chen, S.R.W., Tang, J., et al. (2019). Two pools of IRE1 α in cardiac and skeletal muscle cells. *Faseb. J.* **33**, 8892–8904.
43. Wang, W.-A., and Demaurex, N. (2021). Proteins Interacting with STIM1 and Store-Operated Ca²⁺ Entry. *Prog. Mol. Subcell. Biol.* **59**, 51–97.
44. Jing, J., He, L., Sun, A., Quintana, A., Ding, Y., Ma, G., Tan, P., Liang, X., Zheng, X., Chen, L., et al. (2015). Proteomic mapping of ER–PM junctions identifies STIMATE as a regulator of Ca²⁺ influx. *Nat. Cell Biol.* **17**, 1339–1347.
45. Jennette, M.R., Baraniak, J.H., Zhou, Y., and Gill, D.L. (2022). The unfolding and activation of STIM1 in store-operated calcium signal generation. *Cell Calcium* **102**, 102537.
46. Shaw, P.J., and Feske, S. (2012). Physiological and pathophysiological functions of SOCE in the immune system. *Front. Biosci.* **4**, 2253–2268.
47. Grootjans, J., Kaser, A., Kaufman, R.J., and Blumberg, R.S. (2016). The unfolded protein response in immunity and inflammation. *Nat. Rev. Immunol.* **16**, 469–484.
48. Di Conza, G., Ho, P.-C., Cubillos-Ruiz, J.R., and Huang, S.C.-C. (2023). Control of immune cell function by the unfolded protein response. *Nat. Rev. Immunol.* **23**, 546–562.
49. Silva-Rojas, R., Laporte, J., and Böhm, J. (2020). STIM1/ORAI1 Loss-of-Function and Gain-of-Function Mutations Inversely Impact on SOCE and Calcium Homeostasis and Cause Multi-Systemic Mirror Diseases. *Front. Physiol.* **11**, 604941.
50. He, S., Fu, T., Yu, Y., Liang, Q., Li, L., Liu, J., Zhang, X., Zhou, Q., Guo, Q., Xu, D., et al. (2021). IRE1 α regulates skeletal muscle regeneration through myostatin mRNA decay. *J. Clin. Invest.* **131**, e143737.
51. Barone, V., Del Re, V., Gamberucci, A., Polverino, V., Galli, L., Rossi, D., Costanzi, E., Toniolo, L., Berti, G., Malandrini, A., et al. (2017). Identification and characterization of three novel mutations in the CASQ1 gene in four patients with tubular aggregate myopathy. *Hum. Mutat.* **38**, 1761–1773.
52. Wilson, R.J., Lyons, S.P., Koves, T.R., Bryson, V.G., Zhang, H., Li, T., Crown, S.B., Ding, J.-D., Grimsrud, P.A., Rosenberg, P.B., and Muoio, D.M. (2022). Disruption of STIM1-mediated Ca²⁺ sensing and energy metabolism in adult skeletal muscle compromises exercise tolerance, proteostasis, and lean mass. *Mol. Metabol.* **57**, 101429.
53. Zhu, J., Zhang, X., Xie, H., Wang, Y., Zhang, X., and Lin, Z. (2021). Cardiomycocyte Stim1 Deficiency Exacerbates Doxorubicin Cardiotoxicity by Magnification of Endoplasmic Reticulum Stress. *J. Inflamm. Res.* **14**, 3945–3958.
54. Liang, X., Xie, J., Liu, H., Zhao, R., Zhang, W., Wang, H., Pan, H., Zhou, Y., and Han, W. (2022). STIM1 Deficiency In Intestinal Epithelium Attenuates Colonic Inflammation and Tumorigenesis by Reducing ER Stress of Goblet Cells. *Cell. Mol. Gastroenterol. Hepatol.* **14**, 193–217.
55. Zhang, I.X., Ren, J., Vadrevu, S., Raghavan, M., and Satin, L.S. (2020). ER stress increases store-operated Ca²⁺ entry (SOCE) and augments basal insulin secretion in pancreatic beta cells. *J. Biol. Chem.* **295**, 5685–5700.
56. Hogan, P.G., Lewis, R.S., and Rao, A. (2010). Molecular basis of calcium signaling in lymphocytes: STIM and ORAI. *Annu. Rev. Immunol.* **28**, 491–533.
57. Song, M., Sandoval, T.A., Chae, C.-S., Chopra, S., Tan, C., Rutkowski, M.R., Raundhal, M., Chaurio, R.A., Payne, K.K., Konrad, C., et al. (2018). IRE1 α -XBP1 controls T cell function in ovarian cancer by regulating mitochondrial activity. *Nature* **562**, 423–428.
58. Cubillos-Ruiz, J.R., Bettigole, S.E., and Glimcher, L.H. (2017). Tumorigenic and Immunosuppressive Effects of Endoplasmic Reticulum Stress in Cancer. *Cell* **168**, 692–706.
59. Wang, M., and Kaufman, R.J. (2016). Protein misfolding in the endoplasmic reticulum as a conduit to human disease. *Nature* **529**, 326–335.
60. Urano, F., Wang, X., Bertolotti, A., Zhang, Y., Chung, P., Harding, H.P., and Ron, D. (2000). Coupling of stress in the ER to activation of JNK protein kinases by transmembrane protein kinase IRE1. *Science* **287**, 664–666.
61. Oh-hora, M., Yamashita, M., Hogan, P.G., Sharma, S., Lamperti, E., Chung, W., Prakriya, M., Feske, S., and Rao, A. (2008). Dual functions for the endoplasmic reticulum calcium sensors STIM1 and STIM2 in T cell activation and tolerance. *Nat. Immunol.* **9**, 432–443.
62. Alansary, D., Peckys, D.B., Niemeyer, B.A., and de Jonge, N. (2020). Detecting single ORAI1 proteins within the plasma membrane reveals higher order channel complexes. *J. Cell Sci.* **133**, jcs240358.
63. Hetz, C., Bernasconi, P., Fisher, J., Lee, A.-H., Bassik, M.C., Antonsson, B., Brandt, G.S., Iwakoshi, N.N., Schinzel, A., Glimcher, L.H., and Korsmeyer, S.J. (2006). Proapoptotic BAX and BAK modulate the unfolded protein response by a direct interaction with IRE1 α . *Science* **312**, 572–576.
64. Li, H., Korennykh, A.V., Behrman, S.L., and Walter, P. (2010). Mammalian endoplasmic reticulum stress sensor IRE1 signals by dynamic clustering. *Proc. Natl. Acad. Sci. USA* **107**, 16113–16118.
65. Luik, R.M., Wu, M.M., Buchanan, J., and Lewis, R.S. (2006). The elementary unit of store-operated Ca²⁺ entry: local activation of CRAC channels by STIM1 at ER-plasma membrane junctions. *J. Cell Biol.* **174**, 815–825.
66. Lee, A.-H., Iwakoshi, N.N., and Glimcher, L.H. (2003). XBP-1 Regulates a Subset of Endoplasmic Reticulum Resident Chaperone Genes in the Unfolded Protein Response. *Mol. Cell Biol.* **23**, 7448–7459.
67. Spahn, P.N., Bath, T., Weiss, R.J., Kim, J., Esko, J.D., Lewis, N.E., and Harismendy, O. (2017). PinAPL-Py: A comprehensive web-application for the analysis of CRISPR/Cas9 screens. *Sci. Rep.* **7**, 15854.
68. Brunetti, J., Koenig, S., Monnier, A., and Frieden, M. (2021). Nanopattern surface improves cultured human myotube maturation. *Skeletal Muscle* **11**, 12.
69. Shcherbakova, D.M., and Verkhusha, V.V. (2013). Near-infrared fluorescent proteins for multicolor in vivo imaging. *Nat. Methods* **10**, 751–754.
70. Pusapati, G.V., Kong, J.H., Patel, B.B., Krishnan, A., Sagner, A., Kinnebrew, M., Briscoe, J., Aravind, L., and Rohatgi, R. (2018). CRISPR Screens Uncover Genes that Regulate Target Cell Sensitivity to the Morphogen Sonic Hedgehog. *Dev. Cell* **44**, 113–129.e8.
71. Sepulveda, D., Rojas-Rivera, D., Rodríguez, D.A., Groenendyk, J., Köhler, A., Lebeaupin, C., Ito, S., Urrea, H., Carreras-Sureda, A., Hazari, Y., et al. (2018). Interactome Screening Identifies the ER Luminal Chaperone Hsp47 as a Regulator of the Unfolded Protein Response Transducer IRE1 α . *Mol. Cell* **69**, 238–252.e7.
72. Perez-Riverol, Y., Bai, J., Bandla, C., García-Seisdedos, D., Hewapathirana, S., Kamatchinathan, S., Kundu, D.J., Prakash, A., Frericks-Zipper, A., Eisenacher, M., et al. (2022). The PRIDE database resources in 2022: a hub for mass spectrometry-based proteomics evidences. *Nucleic Acids Res.* **50**, D543–D552.
73. Mi, H., and Thomas, P. (2009). PANTHER Pathway: An Ontology-Based Pathway Database Coupled with Data Analysis Tools. *Methods Mol. Biol.* **563**, 123–140.

STAR★METHODS

KEY RESOURCES TABLE

REAGENT or RESOURCE	SOURCE	IDENTIFIER
Antibodies		
gamma Tubulin	ThermoFisher	4D11, MA1-850; RRID:AB_2211249
anti-STIM1 (N-terminal)	Sigma	S6072; RRID:AB_1079008
anti-beta-Actin	Abcam	ab8227; RRID:AB_2305186
anti-HA (F-7)	Invitrogen	71-5500; RRID:AB_2533988
anti-IRE1 α (B12)	Santa-Cruz	sc-390960; RRID:AB_2927490
anti-IRE1 α	CST	3294; RRID:AB_823545
anti-Lamin A/C	CST	2032T; RRID:AB_2136278
anti-GFP	Sigma	SAB4301138; RRID:AB_2750576
Anti-MyHC: MF-20	DSHB Fischman, D.A	MF 20; RRID:AB_2147781
anti-MEF2C	Cell Signaling	5030S; RRID:AB_10548759
anti-HA (6E2)	CST	2367; RRID:AB_10691311
Anti-Orai1	abcam	AB59330; RRID:AB_943730
anti-HA high affinity	Roche/Sigma	11867423001; RRID:AB_390918
CD4-Percp-cy5.5	Tonbo bioscience	65-0042; RRID:AB_2621876
IL2-PE	BD Biosceicnes	554428; RRID:AB_395386
anti-mouse-HRP	Bio-Rad	1706516; RRID:AB_2921252
Anti-rabbit-HRP	Bio-Rad	1721019; RRID:AB_11125143
Bacterial and virus strains		
Mouse CRISPR Knockout Pooled Library	Addgene	73633-LV
Stable NEB	New England Biolabs	C3040H
Subcloning Efficiency TM DH5 α TM Competent Cells	Invitrogen	18265017
Plenti CaMPARI2 virus	This Study	N/A
PLX-311-Cas9-I720 virus	This Study	N/A
Biological samples		
N/A	N/A	N/A
Chemicals, peptides, and recombinant proteins		
Thapsigargin	Sigma	T9033/CAY10522
Fura2-AM	Invitrogen	F1201
Fluo-8, AM	AAT Bioquest	21082
Biliverdin hydrochloride	Sigma	30891
Hoechst 33342	Thermo-Fisher	H3570
m-3M3FBS	Santa Cruz	sc-202217
L-Glutamic acid γ -(p -nitroanilide) hydrochloride	Santa Cruz	sc-211703
Tunicamycin	Sigma	SML1287
KN-62	Santa Cruz	sc-3560
puromycin	Gibco	A1113803
blasticidin	invivogen	BLL-36-03C
Hygromycin	invivogen	31282-04-9
RIPA buffer	Sigma	R0278-50ML
4% paraformaldehyde	Brunschwig-AlfaAesar,	043368
cOmplete TM , Mini, EDTA-free Protease Inhibitor Cocktail	Roche	04693159001

(Continued on next page)

Continued

REAGENT or RESOURCE	SOURCE	IDENTIFIER
Bovine Serum albumin	Sigma	A3912-100G
Ultra Pure agarose	Invitrogen	16500-500
Milk (Lait ecreme en poudre)	COOP	N/A
Lipofectamine® 2000 Transfection Reagent	Thermo-Fisher	11668019
Dye eFluor 780	ebioscience	ebioscience
NP40/Nonidet™ P 40 Substitute, 4-Nonylphenyl-polyethylene glycol	Sigma	9016-45-9
Poly-L-lysine solution	Sigma	P4832
NuPAGE® LDS Sample Buffer (4X)	invitrogen	NP0007
dithiothreitol	Thermo-Fisher	R0861
TWEEN 20	Sigma	P1379
Cyclopiazonic acid from Penicillium cyclopium	Sigma	c1530

Critical commercial assays

Amata Cell Line Nucleofector Kit T	Lonza	VCA-1002
Duolink	Sigma	DUO92101
RNeasy Mini Kit	Qiagen	74104
QSCRIPT CDNA Supermix	Quantabio	95048-100
Amicon Ultra-15 Centrifugal Filter Unit	Merk-Millipore RT	UFC905024
BCA Protein Assay	Pierce™	23221/23225/23224
MicroBeads L3T4	Miltenyi	130-049-201
Acclaim pepmap100, C18, 3µm, 75 µm × 20 mm nano trap-column	Thermo Fisher Scientific	N/A
TaKaRa Ex Taq® DNA Polymerase	Takarabio	RR001A
JetQuick™ Blood and Cell Culture DNA Midiprep Kit	Thermo	A30703
4-20% Mini-PROTEAN® TGX™ Precast Protein Gels, 10-well, 30 µL	Bio-rad	4561093
iBlot® Transfer Stack, PVDF	Invitrogen	IB401001
SureBeads™ Protein G Magnetic Beads	Bio-rad	1614023
Firefly & Renilla Luciferase Single Tube Assay Kit	Biotium	30081-1
Immobilon Western HRP	Millipore	WBKLS0500

Deposited data

Mass Spectrometry IRE1 WT vs. KO	PRIDE	PXD046579
NGS CaMPARI Screening	ENA	E-MTAB-13548
Uncropped Gels	Mendeley data	10.17632/4zyx9gbhzt.1.

Experimental models: Cell lines

Mouse Embryonic Fibroblast IRE1α-deficient	David Ron, University of Cambridge	Urano et al. ⁶⁰
Mouse Embryonic Fibroblast STIM1 and STIM2 deficient	Dr Masatsugu Oh-hora (Tokyo Medical and Dental University, Tokyo, Japan)	Oh-hora et al. ⁶¹
HEK ORAI123 triple KO	Barbara Nyemeyer, Lab (jcs.240358)	Alansari et al. ⁶²
HEK293T	ATCC	CRL-11268 (Lot n° 59587035)
Jurkat E6.1	ECACC	88042803
Jurkat E6.1 + Cas9 Puro	Demaurex Lab, UNIGE	Carreras Sureda et al. ³¹
Jurkat Crispr Control	This study	4 Clones
Jurkat Crispr IRE1-KO	This study	4 Clones
Mouse Embryonic Fibroblast IRE1α-deficient + IRE1-HA + Cas9 i720	This Study	Pooled population

(Continued on next page)

Continued

REAGENT or RESOURCE	SOURCE	IDENTIFIER
Mouse Embryonic Fibroblast IRE1 α -deficient + IRE1-HA + Cas9 i720 + De Brie Library	This study	Single Clone
Human primary myoblasts derived from healthy donors	Frieden Lab, UNIGE	N/A
Experimental models: Organisms/strains		
Ern1 exon2 floxed mice	Yong, Liu Lab	Shao et al. ³²
Oligonucleotides		
Dox miRNA targeted to STIM1	This study	N/A
Recombinant DNA		
pMSCV IRE1 α -HA-Hygro	Hetz Lab, U Chile	Hetz et al. ⁶³
pMSCV MOCK-Hygro	Hetz Lab, U Chile	Hetz et al. ⁶³
pMSCV IRE1 α -HA-1-300 Hygro	This study	N/A
pMSCV IRE1 α -HA-D123P-Hygro	Hetz Lab, U Chile	Hetz et al. ⁶³
IRE1 α -HA- Δ C	Hetz Lab, U Chile	Hetz et al. ⁶³
IRE1 α -HA- Δ N	Hetz Lab, U Chile	Hetz et al. ⁶³
pCDNA5-IRE1gfp	Peter Walter Lab	Li et al. ⁶⁴
pCMV6-XL5-STIM1-mCherry	Richard Lewis lab	Luik R. M et al. ⁶⁵
pCMV6-XL5-STIM1-mCherry 1-151	This study	N/A
pCMV6-XL5-STIM1-mCherry 1-243	This study	N/A
pLX-311-Cas9	Addgene	96924
CRISPR double nickase control	Santa Cruz	sc-400576-NIC
CRISPR double nickase IRE1	Santa Cruz	sc-437281
pMD2G	addgene	12259
psPAX2	addgene	12260
Hs.Cas9.ERN1.1.AB	IDT	224748420
Hs.Cas9.ERN1.1.AA	IDT	224748419
pENTR1a-tagRFP-KDEL	addgene	11141774177
YC 3.6	Addgene	58182
SPLICS ER-PM long	Addgene	164111
pcDNA3-CaMPARI	Addgene	60421
pLentiCas9-GFP	Addgene	78546
Plenti CAMPARI2	This study	N/A
Plx-311-Cas9-i720	This study	N/A
piRFP720-N1	Addgene	45461
pGL3 2xUPRE-Luc	Glimcher Lab	Lee et al. ⁶⁶
phRL-TK-luc	Promega	N/A
pCDNA3 Empty	Frieden Lab	N/A
NFAT-c1 GFP	Frieden Lab	N/A
pCMV/Myc/ER-GFP	Invitrogen	N/A
Software and algorithms		
PinAPL-Py	UCSD	Spahn et al. ⁶⁷
Flowjo	N/A	N/A
Graph Prism	N/A	N/A
Panther Online Tool	N/A	N/A
Proteome Discoverer 2.4 software	(Thermo Fisher Scientific)	

RESOURCE AVAILABILITY

Lead contact

Further information and requests for resources and reagents should be directed to, and will be fulfilled by Amado Carreras Sureda (amado.carrerassureda@unige.ch).

Materials availability

Plasmids and cell lines generated in this study will be deposited to Addgene and/or are available upon request to the lead author.

Data and code availability

- Data for mass spectrometry proteomics have been deposited to the ProteomeXchange Consortium via the PRIDE partner repository with the dataset identifier PRIDE: PXD046579 and with a doi:10.6019/PXD046579. Likewise, the next-generation sequencing data are available the European Nucleotide Archive, (ENA: E-MTAB-13548). Finally, uncropped gels are deposited on Mendeley Data: <https://doi.org/10.17632/4zyx9gbhzt.1>. These data are publicly available as of the date of publication.
- This paper does not report original code
- Any additional information required to reanalyze the data reported in this paper is available from the [lead contact](#) upon request.

EXPERIMENTAL MODEL AND STUDY PARTICIPANT DETAILS

Human primary myoblasts

Human myoblast samples were obtained after orthopedic surgery (surgical waste) on patients without known muscular diseases and isolated from semitendinous muscle samples. Samples were collected anonymously after obtaining a written consent and approval by the University of Geneva (protocol CCER no. PB_2016-01793 (12–259) accepted by the Swiss Regulatory Health Authorities and approved by the “Commission Cantonale d’Ethique de la Recherche” from the Geneva Cantonal Authorities, Switzerland). Sex and Age were not taken into consideration as every individual had its own control. The purification of myoblasts was performed as in⁶⁸. Cells were expanded in a growth medium (GM). Differentiation was achieved by replacing the GM media for differentiation medium (DM), and stained for primary antibodies after 48–72h. Cellular genetic alterations are described above. A complete description of the composition of these medias can be found here.⁶⁸ When indicated, primary cells were transduced with the viral particles expressing a Doxycycline inducible miRNA targeted to STIM1 and cultured in selection media (blasticidin (20 μ g/ml)) for 6 days. 1 μ M Dox for 72h was used to deplete STIM1 successfully before plating for the indicated experiments. CRISPR double nickase targeted to IRE1 α or scrambled as a control (sc-400576-NIC and sc-437281; Santa Cruz) were transfected in primary cells. After 24h cells were pulsed for 2 days in puromycin and FACS sorted for GFP. Resulting cells were expanded for 1 week before processing for the indicated experiments. Information regarding the gender and age of the healthy human donors is not available.

ERN1 CD4 cre studies

Ern1 floxed mice on exon 2 was previously described in³² and bred with CD4 CRE. IRE1 deletion was confirmed by WB and qPCR. Male animals 4 months old were used for this study. CD4-Cre+ mice were kindly provided as a gift from Prof. Xiao Su (Chinese Academy of Medical Sciences). The mice were housed in the animal facility of Shanghai Jiao Tong University School of Medicine under specific pathogen-free conditions. Animal experiments were conducted in accordance with institutional guidelines approved by the Shanghai Jiao Tong University School of Medicine Institutional Animal Care and Use Committee.

T cells were isolated and enriched using (L3T4) MicroBeads (130-049-201), from Miltenyi, following manufacturer’s instructions as previously described. CD4 T cells were treated with Tg or activated with CD3/CD28 and evaluated by qPCR or FACS staining. For FACS staining, dead cells were excluded using the viability Dye eFluor 780 (ebioscience, 65-0865-14), followed by surface staining with CD4-Percp-cy5.5 (Tonbo bioscience, 65-0042-U100) in PBS containing fetal bovine serum (FBS) plus EDTA for 30min on ice, then washed twice, fixed, permeabilized and labeled with antibody against IL2-PE (BD Biosciences, 554428). Samples were collected on LSRII (BD) flow cytometry and analyzed using FlowJo software.

METHOD DETAILS

Antibodies and reagents

This manuscript used the following reagents; Thapsigargin (T9033/CAY10522, Sigma); Fura2-AM, (F1201, Invitrogen); Fluo-8, AM (21082, AAT Bioquest); Biliverdin hydrochloride (30891, Sigma); Cyclopiazonic acid from Penicillium cyclopium, (c1530, Sigma); Hoechst 33342 (H3570, Thermo-Fisher), m-3M3FBS (sc-202217, Santa Cruz); L-Glutamic acid γ -(p -nitroanilide) hydrochloride (sc-211703, Santa Cruz) KN-62 (sc-3560, Santa Cruz); Tunicamycin (SML1287, Sigma).

Cell culture and stable cell lines

All MEFs or HEK293 cells were maintained in DMEM medium that was supplemented with 5 and 10% fetal bovine serum (FBS) respectively and non-essential amino acids, and grown at 37°C with 5% CO₂. STIM1 and STIM2 DKO MEF cells were generated in.⁶¹ IRE1 α -deficient cells were a kind gift from prof. David Ron⁶⁰ University of Cambridge. HEK-293 cells CRISPR triple knockout for ORA1, 2 and 3 were a kind gift from Dr. Barbara Nyemeier,⁶² University of Saarland. Jurkat T clone E6 cells were purchased from ECACC and grown in RPMI 1640 (21875-034 Life Technologies) supplemented with 10 FCS and 1% Pen/Strep.

IRE1 α -deficient MEFs were stably transduced with retroviral expression vectors for IRE1 α -HA, IRE1 α -D123P-HA, or an empty vector-expressing retrovirus (referred as Mock) were generated as.²² IRE1 α - Δ C-HA, IRE1 α - Δ N-HA were generated in⁶³ while IRE1 1-300-HA was generated in this study by PCR cloning. These constructs, contain two tandem HA sequences at the C-terminal

domain and a precision enzyme site before the HA tag. pCMV6-XL5-STIM1-mCherry plasmid was a kind gift from Prof. Richard Lewis.⁵⁵ This plasmid was mutagenized to an STOP codon on STIM1 amino acid 214 or 154 by PCR mutagenesis.

CRISPR Jurkat cells were generated for this study by stably expressing with lentiviral particles pLX-311-Cas9 construct (Addgene 96924)³⁵ and transiently transfecting with Amaxa Cell Line Nucleofector Kit T (Ref: VCA-1002, Lonza) two sets of sgRNAs (Hs.Cas9.ERN1.1.AB ref. 224748420/Hs.Cas9.ERN1.1.AA ref. 224748419, IDT). Single clone sorting, genomic DNA sequencing and Western blot were used to validate KO cells. Two different sets of clones were prepared and a minimum of four clones (control and IRE1 α , for each set) were screened for *XBP1* mRNA splicing and the upregulation of BIP and CHOP (after experimental ER stress). Alternatively, for human primary myoblasts we used CRISPR double nickase targeted to IRE1 α or scrambled as a control (sc-400576-NIC and sc-437281; Santa Cruz). Myoblasts were pulsed with puromycin (2 μ g/ml) for 2 days after transfection and sorted based on fluorescence to then be amplified.

MEF-IRE1KO re-expressing IRE1-HA or Mock were also infected with PLX311-Cas9i720 and Plenti Campari2, which were generated for this work and available upon request. Briefly, lentiviral expression vectors were co-transfected with pMD2G/psPAX2 into HEK-293T cells to produce viral particles.³¹ After accumulation (Amicon) and filtration of the virus these were stored at -80°C .

All cells sorted in this study were generated using a Beckman Coulter MoFlo Astrios integrated in PSL2 hood. All cell lines from this study were tested negative for mycoplasma contamination. Jurkat, HEK 293 and MEF cells are listed as commonly misidentified cell lines maintained by the International Cell Line Authentication Committee. In our hands, HEK 293T cells were genetically confirmed (by genomic profiling [STRs]) prior to stockage and Jurkat E6.1 cells were purchased from ECACC (ref number 880442803).

Western blot analysis

Cells were collected and homogenized in RIPA buffer (20 mM Tris pH 8.0, 150 mM NaCl, 0.1% sodium dodecyl sulfate (SDS), 0.5% Triton X-100) containing a protease inhibitor cocktail (Roche). Protein concentration was determined by micro-BCA assay (Pierce), and 50–100 μ g of total protein was loaded onto SDS–polyacrylamide gel electrophoresis mini gels (Bio-Rad Laboratories) before transfer onto polyvinylidene difluoride (PVDF) membranes. Membranes were blocked using PBS, 0.02% Tween 20, 5% milk for 1 h at room temperature, then probed with the following primary antibodies; gamma Tubulin (4D11) (MA1-850, ThermoFisher), anti-STIM1 (N-terminal) (S6072, Sigma), anti-beta-Actin (ab8227 Abcam), anti-GFP (SAB4301138, Sigma), anti-HA (715500, Invitrogen), anti-IRE1 α (sc-390960, Santa-Cruz; and/or 3294, CST), anti-Lamin A/C (2032T, CST). Secondary antibodies were anti-mouse-HRP, and rabbit-HRP (1706516 and 172101, Bio-Rad (USA).

Immunofluorescence, protein ligation assays and TIRF

For PLA and immunofluorescence assays, cells were seeded on 12 mm cover slips with no coating. After transfection and/or and treatment (as indicated), cells were fixed for 20 min at room temperature using 4% paraformaldehyde (Brunschiwig-AlfaAesar, ref. 043368) and then permeabilized using 0.1% NP-40 in PBS containing 0.5% bovine serum albumin (BSA) for 10 min. Blocking was performed for 1 h using 5% FBS in PBS containing 0.5% BSA, cells were incubated with the indicated antibodies (also for PLA), MyHC: MF-20 (MF 20 was deposited to the DSHB by Fischman, D.A. (DSHB Hybridoma Product MF 20), anti-MEF2C (5030S, Cell Signaling), anti-HA (2367, CST), anti-IRE1 α (B-12) (sc-390960, Santa Cruz Tech.), Anti-Orai1 antibody (AB59330, abcam), anti-STIM1 (N-terminal) (S6072, Sigma), overnight at 4°C followed by either staining with Alexa-conjugated secondary antibodies (Thermo-Fischer) or following Duolink manufacturer's instructions as previously described (Duolink, Sigma-Aldrich). Images were obtained in a LSM700 Zeiss Axio Imager M2 microscope. MEF cells either DKO6 (S1/S2 DKO) or IRE1-KO reconstituted with mock or IRE1-HA were transfected with SPLICS to report ER-PM, STIM1-cherry, IRE1-GFP or KDEL GFP enrichment to the PM. Cells were seeded 24h after transfection in 35mm coverslips and imaged 24h after in a modified Ringer's solution. To observe ER/PM accumulation over time cells were bathed with Tg 1 μ M and imaged every 20 s in calcium-containing solution where Tg 1 μ M was added after 1 min of recording. TIRF setting consisted on Nikon Eclipse Ti microscope equipped with a Perfect Focus System (PFS III) using a 100 \times oil CFI Apochromat TIRF Objective (NA 1.49; Nikon Instruments Europe B.V.). GFP was imaged using ZET488/10 excitation filter (Chroma Technology Corp.). Cherry/RED images were obtained using ZET 561/10 excitation filter (Chroma Technology Corp., Bellows Falls, VT). All experiments were performed at room temperature (22°C – 25°C) All emission signals were collected by a cooled EMCCD camera (iXon Ultra 897, Andor Technology Ltd).

Immunoprecipitation

HA-tagged IRE1 was immunoprecipitated by incubating protein extracts in an IP buffer (0.5% NP-40, 250 mM NaCl, 30 mM Tris, 0.5% glycerol, pH 7.4, and protease inhibitors) with 5 μ L/sample of magnetic beads (1614013, Biorad) to preclear the samples to then add a rat Anti-HA High Affinity antibody (0.25 μ g/ μ L 11867423001, Roche (0.5 μ g in 400 μ L) overnight at 4°C under rotation. The day after we added 20 μ L of prewashed magnetic beads (1614013, Biorad) for 3 h at 4°C . Beads were subsequently washed for 5 min once with IP buffer, two times with IP buffer with 500 mM NaCl and a last wash with IP buffer. Protein complexes were eluted by heating at 95°C for 5 min in diluted (1:2) loading buffer with 100 mM dithiothreitol (DTT). Immunoprecipitated samples were assayed in Western blot as indicated.

Calcium measurements using FURA2, Fluo4 and FDSS

Single-cell live imaging calcium assays in MEF-IRE1KO + Mock or +IRE1-HA or HEK (WT or TKO) were performed in.³¹ Briefly, cells were transfected with the indicated constructs or treated (when indicated necessary) and seeded on a 35mm coverslip without (MEF cells) or with Poly-L lysine-coating (HEK). To measure calcium cells were either transfected with YFP Cameleon 3.6 (YC 3.6, a gift from Michael Davidson (Addgene plasmid # 58182)) calcium FRET sensor or loaded with 2 μ M Fura-2-AM, in modified Ringer's for 25 min at room temperature (RT). yc3.6 FRET was measured with CFP and FRET settings where both were excited at 440 and CFP emission measured at 480 ± 40 while FRET channel at 525 ± 40 . For Fura a 340/380 nm excitation and 510 ± 40 nm emission ratiometric imaging was performed every 2 s. Manganese quench experiments were performed using a 360nm filter excitation measuring at 510 ± 40 nm emission. 3M3FBS, Manganese and Tg (either at 25nM or 1 μ M) were used as stimuli in the presence of 1mM Calcium of extracellular solution. SOCE was also measured using a two-step protocol triggered by emptying the ER stores with Thapsigargin 1 μ M or Ciclopiazonic acid 10 μ M in a Ca^{2+} -free solution containing 1 mM EGTA instead of 2 mM $CaCl_2$. Extracellular calcium re-addition revealed SOCE activity.

Calcium experiments measured by flow Cytometry on Jurkat cells were executed by incubating 0.5 million cells in 0.5mL with Fluo-4 (2 μ M 30 min, RT) and washed for 15 min in a calcium containing solution. BD Accuri C6 with a flow set of 1 μ L per second was used. Every experiment started with 5×10^5 cells in 510 μ L of calcium-free solution (1 mM EGTA). After 1 min 50 μ L of Tg 10 μ M was added to empty ER stores. After 300 s, we added 100 μ L of $CaCl_2$ (Final concentration 2.5 mM) to reveal SOCE.

Hit validation was achieved using FDSS hamamatsu setup in the READS facility at UNIGE or CaMPARI photoconversion (see next section). Briefly, 15.000 cells/well were seeded in a 396 well plate 24h prior to experiment, incubated with Fluo-4 5 μ M for 30 min at RT in Calcium containing solution. After washing out wells were image din 40 μ L of cf., 10 μ L og Tg 5 μ M was added (cf. = 1 μ M) to evoke ER leak and calcium re addition consisted on 25 μ L of 8mM $CaCl_2$.

Luciferase measurements

MEF DKO S1/S2 cells were transiently transfected with pGL3 2xUPRE-Luc plasmid together with a control plasmid encoding the Renilla luciferase (phRL-TK-luc, Promega) and STIM1 or PCDNA3 were used for luciferase assays (4:1:3 ratio). After 48h cells were treated with Tg 100nM for the indicated times and processed with a Firefly & Renilla Luciferase Single Tube Assay Kit (Biotium) and measured in a SpectraMax L 384 w (Molecular devices).

CAMPARI calcium measurements

CAMPARI1 or 2 were first used in single cell microscopy transiently transfected or stably expressed in HEK-WT vs. TKO or the indicated MEF cells. Cells were seeded into 35mm coverslips the day before experiment and imaged using GFP (488ex/520 em) and RFP (560ex/600em) settings. Cells were bathed in modified Ringer's and Photoactivation was achieved by exposing the field of view for the indicated times with 405 light. GFP and RFP channels were measured before and after PC during the indicated protocols to establish PC rate.

FACS measurement of CAMPARI2 in MEF stable expressing cells was achieved by exposing cells to PC light using a home made CaMPARI setup composed of: a CHOLIS 6-LED High power Source (ThorLabs) with 360, 385 and 420 nm lines at 100% rendering 150 mW/cm² maximal output. Cells were exposed to CPA 10 μ M or Tg 1 μ M in CF solution (1mM EGTA) for 5 min and then exposed to PC for the indicated times and PC power with the indicated extracellular re-addition. Cells were then trypsinized and placed into FACS tubes to measure 488 to 555 PC in a BDLSR Fortessa unit. Not PC and PC in 1mM EGTA were always used for each experiment in order to define PC. Sytox blue counter staining was used to exclude dying cells.

CAMPARI2 CRISPR screening

CAMPARI1 and 2 were a kind gift from prof. Eric R Schreiter. CAMPARI2 was subcloned into a pLentiCas9-GFP (Addgene: 78546)⁶⁵ by substituting Cas9-gfp for CAMPARI2 insert. In parallel, we used the Cas9-GFP insert and generated a Cas9-i720 by substituting the GFP for iRFP720 far red protein (Addgene: 45461)⁶⁹ at the C terminus of Cas-9 in a PLX-311-Cas9 (Addgene 96924).³⁵ These two plasmids were used to generate lentiviral particles. After transduction of MEF IRE1KO + IRE1-HA cells, and blasticidin selection (5 μ g/ml), single clones positive for Cas9-i720 and CAMPARI2 were selected and infected with the de Brie CRISPR library (Addgene #73633)³⁵ which targets each of 19.674 mouse genes with 4 short guide RNAs. We based our protocol on.⁷⁰ Briefly we spin-infected 180 milion cells with a MOI of 0.4 (10 μ g/ml Polybrene) to introduce the library in our cell line aiming to achieve 600-fold representation of each sgRNA. After selection and expansion for 7 to 10 days with 2.5 μ g/ml of blasticidin and puromycin we froze all cells in aliquots of 9 millions/vial. For each screening 4 vials were thawed and expanded for 1 passage before PC and FACS sorting of 60 milion cells/condition. CAMPARI2 PC for screening was performed in 60 mm plates by lighting with 365, 385 420 nm Led light (Cholis High-Power Led source (Thorlabs) for 3 min at 25 mW/cm². We then FACS sorted the low 10% photoconverted cells, expanded them for 1 week (to achieve 5×10^7 cells) and isolated their genomic DNA using JetQuick Blood and Cell Culture DNA Midiprep Kit (A30703, Thermo). gDNA was amplified using a two step PCR. First PCR used all the gDNA in different reactions using Fw: AAT GGA CTA TCA TAT GCT TAC CGT AAC TTG AAA GTA TTT CG and Rv: TCT GCT GTC CCT GTA ATA AAC CCG AAA ATT TTG AA primers. PCR products were pooled and 10 μ L were used in a 100 μ L final reaction PCR using barcoded P5 and P7 primers as described on³⁵ and sequenced using HiSeq 4000 (Illumina, San Diego, CA, USA) at the iGE3 Genomics platform at the University of Geneva.

RNA isolation, PCR and qPCR

RNA isolation was performed using miniprep RNeasy Mini Kit (ref. 74104, Qiagen). cDNA was obtained using QSCRIPT CDNA Supermix (95048-100, Quantabio). Semi-quantitative PCR primers for the mouse and human *XBP1* and human mRNA splicing were as follows: 5'-AAGAACACGCTTGGGAATGG-3' and 5'-CTGCACCTGCTGCGGAC-3' and 5'-CCTGGTTGCTGAAGAGGAGG-3' and 5'-CCATGGGGAGATGTTCTGGAG-3'. The full description of this assay was described previously.⁷¹ Human and mouse qPCR primers are described in Table S4.

NFAT translocation assays

NFAT-c1 plasmid was a kind gift from Stephan Konig. This was transiently transfected in the indicated lines and treated with Tg1 μ M for 30 60 or 120 min. Images were obtained with and imaged in a LSM700 Zeiss Axio Imager M2 microscope. Biochemical translocation analysis were performed by isolating nuclear vs. cytosolic fractions by rapid isolation of Nuclei from cells *in Vitro*.⁶²

LC/MS studies

Biological replicates of IRE1-KO and IRE1-KO + IRE1-HA re-expressing MEF cells were used for this analysis. Samples were prepared in the Proteomic platform (UNIGE). Briefly, after lysis and trypsinization, and labeling of all samples, these were pooled together and injected (1 μ g) in an LC-ESI-MS/MS (Orbitrap Fusion Lumos Tribrid mass spectrometer (Thermo Fisher Scientific)) equipped with an Easy nLC1200 liquid chromatography system (Thermo Fisher Scientific). Peptides were trapped (Acclaim pepmap100, C18, 3 μ m, 75 μ m \times 20 mm nano trap-column (Thermo Fisher Scientific)) and separated on a home made column (75 μ m \times 500 mm, C18 ReproSil-Pur from Dr. Maisch GmbH, 1.9 μ m, 100 \AA). Separation was run for 180 min using a gradient of H₂O/FA 99.9%/0.1% (solvent A) and CH₃CN/H₂O/FA 80.0%/19.9%/0.1% (solvent B). Data-Dependent Acquisition (DDA) was performed with MS1 full scan at a resolution of 120'000 FWHM followed by as many subsequent MS2 scans on selected precursors as possible within 3 s maximum cycle time. MS1 was performed in the Orbitrap with an AGC target of 4x10⁵, a maximum injection time of 50 ms and a scan range from 375 to 1500 m/z. MS2 was performed in the Orbitrap at a resolution of 30'000 FWHM using higher-energy collisional dissociation HCD at 38% NCE. Isolation windows was at 0.7 u with an AGC target of 5x10⁴ and a maximum injection time of 54 ms. A dynamic exclusion of parent ions of 60 s with 10 ppm mass tolerance was applied. Raw data was processed using Proteome Discoverer 2.4 software (Thermo Fisher Scientific). The abundances were normalised on "Total Peptide Amount" and then scaled with the "On all Average" parameter. The protein ratios were directly calculated from the grouped protein abundances and associated p values were calculated with ANOVA test based on the Abundances of individual proteins or peptides. Hits were considered based on significance and a 0.67–1.4 difference in ratio abundance. The mass spectrometry proteomics data have been deposited to the ProteomeXchange Consortium via the PRIDE⁷² partner repository with the dataset identifier PXD046579 and 10.6019/PXD046579.

QUANTIFICATION AND STATISTICAL ANALYSIS

Results were tested for significance using the Kruskal-Wallis ANOVA for unpaired groups followed by multiple comparison post-tests (Bonferroni Multiple Comparison Test, Dunnet or SidaK as stated in the text). Student's t-test was performed for unpaired or paired groups, also one or two tailed experiments are indicated on each figure legend. In all plots p values are indicated: Analysis was performed using GraphPad software. Data analysis for LC/MS were performed using Panther online tool.⁷³ CRISPR genome wide screening analysis was performed using PinAPL-Py:A⁶⁷ using SUMLFC as gene ranking and a Bonferroni p value test. For Tunica-mycin over NT studies only sgRNAs with more than 2 hits over 35x enrichment were considered.